et al., 2000b; Wellman and Nelson, 2003; Fernández-Fernández et al., 2004).

Agents that enhance BK channel activity (BK channel openers) may therefore be effective in protecting neurons from damage following an ischemic stroke and/or in suppressing excess activity of smooth muscle tissues (Lawson, 2000). Many compounds that were found from natural products or were synthesized have been reported to be BK channel openers (Coghlan et al., 2001). Most of these BK channel openers, including BMS-204352 (Gribkoff et al., 2001), are not highly potent activators (EC_{50} values >300 nM) under the resting cellular conditions where intracellular Ca^{2+} concentration is 50 to 150 nM (Schrøder et al., 2003). Terpenoids derived from natural products—dehydrosoyasaponin-I, maxikdiol, and L-735,334—have been reported as BK channel openers (Kaczorowski and Garcia, 1999). In addition, 17β-estradiol (Valverde et al., 1999) and epoxyeicosatrienoic acids (Fukao et al., 2001) may be endogenous BK channel openers, and some transmitters and hormones can enhance BK channel activity via kinase activation (Vergara et al., 1998).

In our previous study (Imaizumi et al., 2002), novel compounds, including pimaric acid, were discovered from terpenoids, which have chemical structures similar to that of maxikdiol, a moderate BK channel opener (Singh et al., 1994). Moreover, our recent study (Ohwada et al., 2003) has revealed that chemical modification of abietic acid, an inactive compound of resin acid derivatives, to dehydroabietic acid resulted in BK channel opening, and further chemical modification to 12,14-dichlorodehydroabietic acid (diCl-DHAA) led to finding of a potent BK channel opener. However, the underlying mechanisms of diCl-DHAA-induced activation of BK channel and the selectivity against voltage-dependent Ca^{2+} (CaV) channel have not been defined. The present study was therefore undertaken to identify molecular mechanisms of diCl-DHAA-induced activation of BK channels and to examine the selectivity against inhibition of CaV channels by using human embryonic kidney (HEK) 293 cells as an expression system.

Materials and Methods

Vector Constructs, Cell Culture, and Transfection. Restriction enzyme-digested DNA fragments of BKα (KpnI/XbaI-double digested) and BKβ1 (EcoRI/XbaI-double digested) were ligated into mammalian expression vectors pcDNA3.1(+) and pcDNA3.1/Zeo(+) (Invitrogen, Carlsbad, CA), respectively, using the TaKaRa ligation kit version 1 (TaKaRa, Osaka, Japan) (Yamada et al., 2001). HEK293 cell lines were obtained from Health Science Research Resources Bank (Tokyo, Japan) and maintained in minimal essential medium (Invitrogen) supplemented with 10% heat-inactivated fetal calf serum (JRH Biosciences, Lenexa, KS), 100 units/ml penicillin (Wako Pure Chemicals, Osaka, Japan), and 100 μg/ml streptomycin (Meiji Seika, Tokyo, Japan). Stable expression of BKα and BKβ was achieved by using calcium phosphate coprecipitation transfection techniques as reported previously (Imaizumi et al., 2002). G418- and G418/zeocin-resistant cells were selected as those which were BKα-expressing and BKβ1-coexpressing, respectively.

The cDNAs encoding voltage-dependent Ca^{2+} channel α1C subunit of the rabbit (rCaVα1C) and β3 subunit of the mouse (mCaVβ3) were kind gifts from Dr. Veit Flockerzi (Institut für Pharmakologie und Toxikologie, Universität des Saarlandes, Hamburg, Germany) and were ligated into mammalian expression vectors pcDNA3.1(+) and pTracer(+), respectively (Murakami et al., 2003). These plasmid vectors were transfected into HEK293 cells for transient expression. The functional coexpression of rCaVα1C and mCaVβ3 was successfully determined by the appearance of the inward currents and green fluorescent protein fluorescence.

Solutions. The standard HEPES-buffered solution for electrophysiological recording had an ionic composition of 137 mM NaCl, 5.9 mM KCl, 2.2 mM $CaCl_2$, 1.2 mM $MgCl_2$, 14 mM glucose, and 10 mM HEPES. The pH of the solution was adjusted to 7.4 with NaOH. The pipette solution for whole-cell recordings of K^+ currents contained 140 mM KCl, 1 mM $MgCl_2$, 10 mM HEPES, 2 mM Na_2ATP, and 5 mM EGTA. The pCa and pH of the pipette solution were adjusted to 6.5 and 7.2 by adding $CaCl_2$ and KOH, respectively. For recordings of single BK channel currents in the excised inside-out patch configuration, the pipette solution contained the standard HEPES-buffered solution or K^+-rich HEPES-buffered solution that was prepared by replacement of 134.1 mM NaCl in the standard HEPES-buffered solution with equimolar KCl. The bathing solution contained 140 mM KCl, 1.2 mM $MgCl_2$, 14 mM glucose, 10 mM HEPES, and 5 mM EGTA. Selected pCa of the bathing solution was obtained by adding adequate amount of $CaCl_2$, and the pH was adjusted to 7.2 with NaOH. The pipette solution for whole-cell recording of Ca^{2+} inward currents had an ionic composition of 140 mM CsCl, 1 mM $MgCl_2$, 10 mM HEPES, 2 mM Na_2ATP, and 5 mM EGTA. The pH of the pipette solution was adjusted to 7.2 by adding CsOH.

Electrophysiological Experiments. The whole-cell and inside-out patch clamps were applied to single cells using CEZ-2400 amplifier (Nihon Kohden, Tokyo, Japan) and EPC-7 amplifier (List Electronics, Darmstadt, Germany), respectively. The procedures of electrophysiological recordings and data acquisition/analysis for whole-cell recording have been described previously (Imaizumi et al., 1989). The resistance of the pipette was 1.5 to 3 MΩ for whole-cell and 15 to 25 MΩ for inside-out patch configurations when filled with the pipette solutions. The series resistance was partly compensated electrically under whole-cell voltage clamp. Whole-cell and single channel recordings were carried out at room temperature (24 ± 1°C). Single channel current analyses were done using software PAT V7.0C (developed by Dr. J. Dempster, University of Strathclyde, Glasgow, Scotland). The open probability (P_o) was measured from the event histogram plotted against current amplitude. The number of channels in a patch was determined from recordings at pCa = 3.5, and the analyses were performed only when the number of channels in a patch was less than six.

Chemicals. Most of pharmacological agents were obtained from Sigma-Aldrich (St. Louis, MO), unless mentioned otherwise. Iberiotoxin was obtained from Peptide Institute Inc. (Osaka, Japan). Pimaric acid, abietic acid, dehydroabietic acid, and diCl-DHAA were obtained from Helix Biotech (New Westminster, BC, Canada). The test compounds were dissolved with dimethyl sulfoxide. The final concentration of dimethyl sulfoxide was 0.03% or lower.

Statistics. Data are expressed as means ± S.E.M. Statistical significance between two groups and among multiple groups was evaluated using Student's *t* test and Scheffé's test after F-test or one-way analysis of variance, respectively.

Results

Effects of diCl-DHAA on Macroscopic BK Channel Currents. Effects of diCl-DHAA on BK channel currents were examined in single HEKBKαβ1 under whole-cell voltage-clamp mode. The Ca^{2+} concentration in the pipette solution was fixed at pCa = 6.5 using a Ca^{2+}-EGTA buffer (see *Materials and Methods*). Depolarization from −60 to +10 mV induced outward currents in both native HEK and HEKBKαβ1, whereas the current density was approximately 4 times larger in the latter cells as reported previously (Imaizumi et al., 2002). Application of diCl-DHAA in a concentration range of 0.1 to 1.0 μM increased the outward

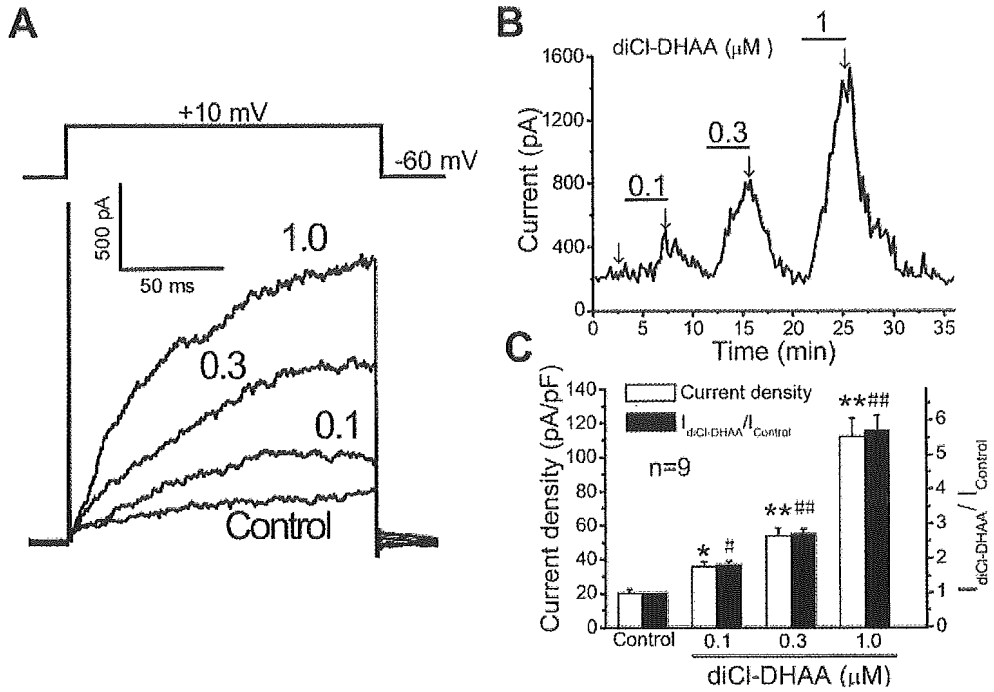

Fig. 1. Effects of diCl-DHAA on macroscopic membrane currents in HEKBK$\alpha\beta$1. A and B, a single HEKBK$\alpha\beta$1 was depolarized from −60 to +10 mV for 150 ms under whole-cell voltage-clamp mode. diCl-DHAA was applied in a concentration range of 0.1 and 1 μM. Original current recordings at different concentrations were superimposed and are shown in A. The peak outward current amplitude at +10 mV was measured and plotted against time in B. The original traces were obtained at the time indicated by vertical arrows in the time course. It is notable that effects of 0.1 to 1 μM diCl-DHAA were completely removed by washout. C, concentration-response relationships for diCl-DHAA. Experiments were carried out in a manner typically shown in A. Data about current density at +10 mV, which was obtained by dividing peak current amplitude with cell capacitance in each cell (pA/pF), are summarized as open columns. The relative amplitude of peak outward current at +10 mV in the presence of diCl-DHAA ($I_{diCl\text{-}DHAA}/I_{control}$) was also determined by taking the amplitude in the absence of diCl-DHAA as unity (closed columns). Means ± S.E.M. are shown by columns and vertical bars, respectively. */#, $p < 0.05$ and **/##, $p < 0.01$ versus control.

currents in HEKBK$\alpha\beta$1 in a dose-dependent manner (Fig. 1, A and B) but not in native HEK cells (data not shown). The enhancement of the outward currents in HEKBK$\alpha\beta$1 was completely removed by washout of diCl-DHAA (Fig. 1B). The relationship between concentrations of diCl-DHAA and corresponding responses is summarized in Fig. 1C. The increase in outward current density by diCl-DHAA was significant at a concentration of 0.1 μM and higher. Taking the current density at +10 mV in the control as unity, the relative amplitude of peak outward currents in the presence of 0.1, 0.3, and 1 μM diCl-DHAA was also plotted against concentration (Fig. 1C).

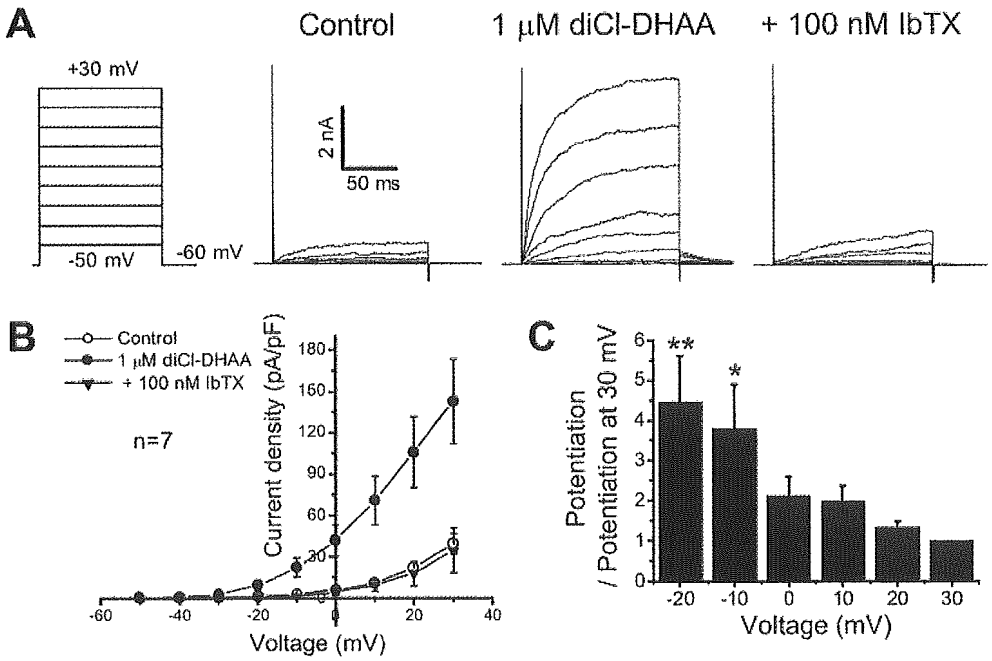

Fig. 2. Effects of diCl-DHAA on I-V relationship in BK$\alpha\beta$1. A, each single HEKBK$\alpha\beta$1 was depolarized from −60 mV by 10-mV steps for 150 ms under whole-cell voltage-clamp mode. The outward currents elicited by depolarization was markedly enhanced by application of 1 μM diCl-DHAA and then reduced by the addition of 100 nM iberiotoxin. B, I-V relationships were obtained in the control (open circles), in the presence of diCl-DHAA (closed circles), and after the addition of 100 nM iberiotoxin (closed triangles) in experiments such as typically shown in A. Number of examples is seven. C, voltage dependence of the potentiation of BK channel current by diCl-DHAA was reevaluated from the data shown in B. The relative potentiation of the outward currents by 1 μM diCl-DHAA was plotted against test potentials by taking that at +30 mV as unity. *, $p < 0.05$ and **, $p < 0.01$ versus unity at +30 mV.

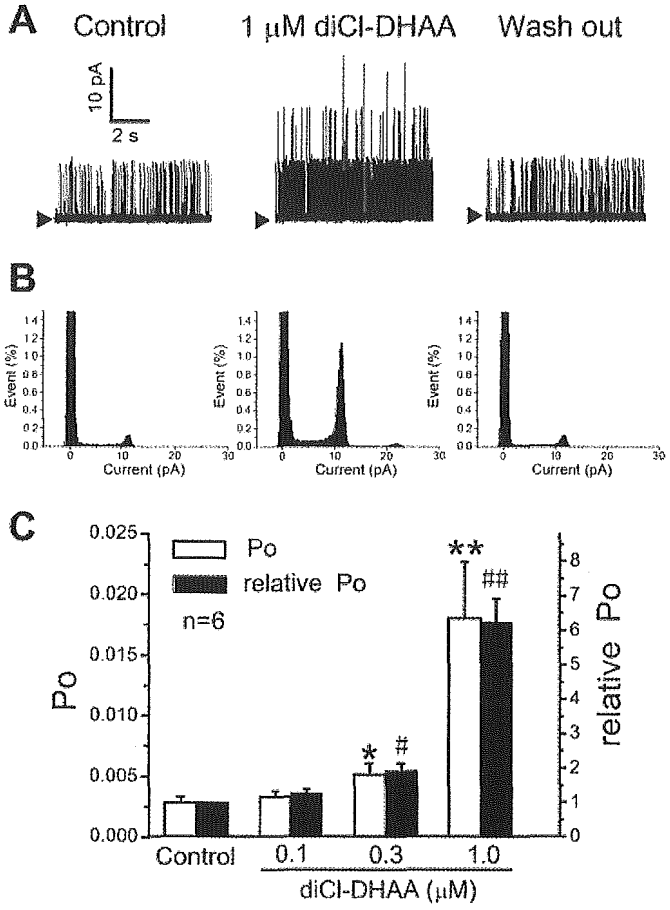

Fig. 3. Effects of diCl-DHAA on single BKα channel currents recorded using an inside-out patch-clamp techniques. A, single channel currents were recorded at +40 mV in a patch from HEKBKα under symmetrical 140 mM K^+ conditions. The free Ca^{2+} in the bathing solution was adjusted to pCa = 7.0. The original current traces were recorded before and after application of 1 μM diCl-DHAA and after the washout of diCl-DHAA. A closed triangle on the left side of each trace indicates the zero current level. B, amplitude histograms in the control, in the presence of 1 μM diCl-DHAA, and after the washout were obtained from the recordings shown in A. The ordinate expresses the relative area (percentage) at the corresponding amplitude in each bin (0.2 pA). C, summarized data demonstrate the relationship between concentrations of diCl-DHAA and P_o of BKα. P_o was calculated from the histogram shown in B as the relative time spent at open state based on the total number of BKα channels in the patch, which was determined by elevating Ca^{2+} concentration to pCa = 3.5 (open columns). The relative P_o was obtained taking the P_o in the absence of diCl-DHAA as unity (closed columns). Number of examples is six. */#, $p < 0.05$ and **/##, $p < 0.01$ versus control.

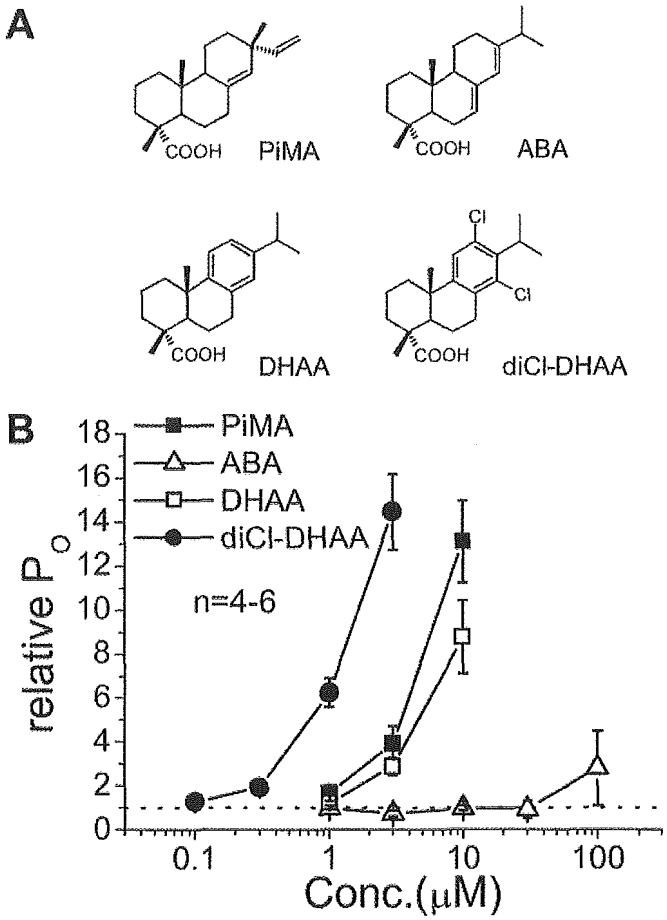

Fig. 4. Structure-activity relationships of abietic acid derivatives on P_o of BKα. A, chemical structures of test compounds pimaric acid, abietic acid, dehydroabietic acid, and diCl-DHAA. B, concentration-response relationships for compounds listed in A. Effects of abietic acid (open triangles), DHAA (open squares), and diCl-DHAA (closed circles) were examined in experiments identical to that shown in Fig. 3 for diCl-DHAA. The data for pimaric acid (closed squares) are taken from a previous study (Imaizumi et al., 2002). The relative P_o was determined taking the P_o in the absence of compounds as unity (a dotted line). Means ± S.E.M. are shown by symbols and vertical bars, respectively. Number of experiments is four to six for each compound.

Voltage Dependence of diCl-DHAA-Induced Enhancement of BK Channel Currents. In Fig. 2, the voltage-dependent enhancement of BK channel currents was examined by analyzing effects of diCl-DHAA on the current-voltage (I-V) relationship. HEKBKαβ1 was depolarized from a holding potential of −60 mV to test potentials in the range between −50 and +30 mV with 10-mV steps (Fig. 2A). Application of 1 μM diCl-DHAA increased the currents at any test potential. Addition of 100 nM iberiotoxin, a specific BK channel blocker, removed the enhancement of outward currents, supporting that the action of diCl-DHAA was selective to BK channel currents. Figure 2B summarizes the relationships between current density of peak outward currents and test potentials in the absence and presence of 1 μM diCl-DHAA and after addition of 100 nM iberiotoxin. The current density at +30 mV was increased from 39.13 ± 7.34 to 142.55 ± 30.81 pA/pF ($n = 7$; $p < 0.01$). In Fig. 2C, the voltage dependence of diCl-DHAA-induced enhancement of BK channel currents was determined as the relationship between the relative potentiation of outward currents and test potentials by taking the potentiation at +30 mV in the presence of 1 μM diCl-DHAA as unity. The potentiation at −20 and −10 mV was significantly greater than that at +30 mV (4.48 ± 1.15 and 3.80 ± 1.09 times at −20 and −10 mV, respectively, $p < 0.01$, versus unity at +30 mV).

Activation of Single BKα Channel Current by diCl-DHAA and Related Compounds. Effects of diCl-DHAA on single BKα channel currents were examined in excised inside-out patch configuration. The bathing and pipette solution contained symmetrical 140 mM K^+. The free Ca^{2+} concentration in the bathing solution was pCa7. Under these conditions, the unitary current amplitude and open probability (P_o) at +40 mV was 10.1 ± 0.2 pA and 0.0028 ± 0.0005 ($n = 6$), respectively. The application of 1 μM diCl-DHAA increased channel activity without change in the unitary

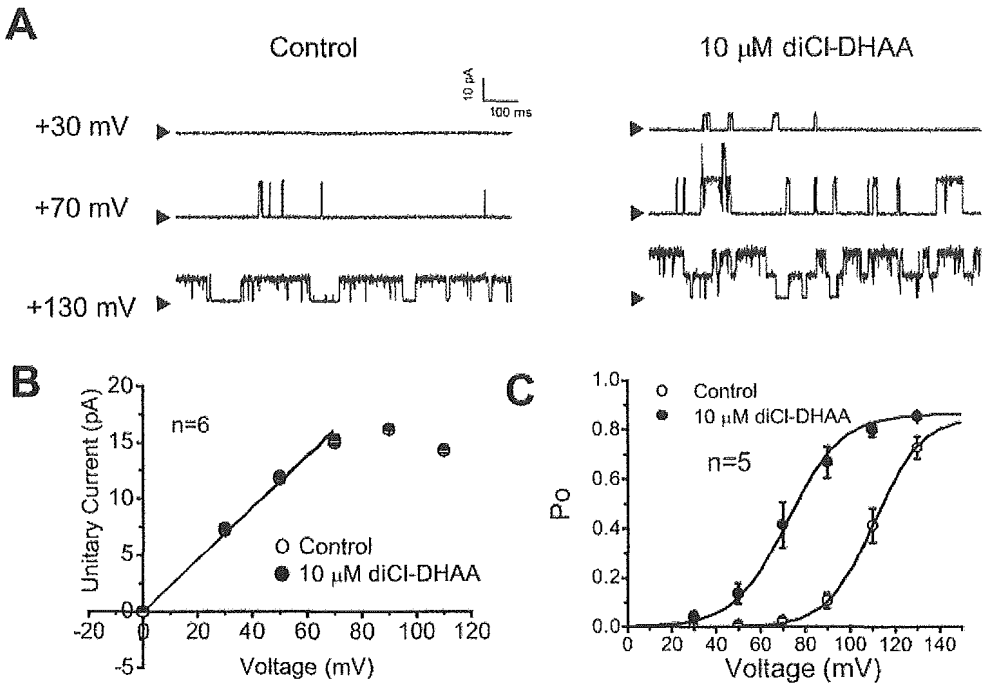

Fig. 5. Effects of diCl-DHAA on single channel conductance and voltage dependence of BKα. Single channel currents of BKα were recorded in inside-out patch configuration at pCa = 7.0 in symmetrical 140 mM K^+ conditions. Recordings were obtained at several test potentials in the range of 0 to +130 mV in the absence and presence of 10 μM diCl-DHAA. Experimental conditions, except applied potentials, are the same as those shown in Fig. 3. A, original current traces at +30, +70, and +130 mV in the absence (left) and presence of 10 μM diCl-DHAA (right). B, relationship between unitary current amplitude and test potentials was plotted in a range of 0 and +70 mV in the absence (open circles) and presence of 10 μM diCl-DHAA (closed circles) and was fitted by a linear line. The single channel conductance was determined from the slope (n = 6). C, effects of diCl-DHAA on voltage dependence of BKα. The relationships between P_o and test potentials were obtained in the absence (open circles) and presence of 10 μM diCl-DHAA (closed circles). Number of examples is five for each. The data were fitted using the Boltzmann equation (see "Results"). The fitted lines are based on the following values of $V_{1/2}$, S, and C: 110.7 mV, 10.5 mV, and 0.15 in the absence and 72.3 mV, 12.2 mV, and 0.13 in the presence of 10 μM diCl-DHAA, respectively.

current amplitude (10.43 ± 0.28 pA, 0.0180 ± 0.0047, n = 6; Fig. 3, A and B). It is notable that diCl-DHAA was effective on BKα even when applied to the cytosolic phase. This effect of diCl-DHAA was completely removed by the washout. The P_o was significantly increased by diCl-DHAA at 0.3 μM and higher concentrations (Fig. 3C), and the relative P_o determined by taking P_o in the control as unity was 1.26 ± 0.13, 1.92 ± 0.19, 6.24 ± 0.67, and 14.45 ± 1.72 in the presence of 0.1, 0.3, 1.0, and 3.0 μM diCl-DHAA, respectively (n = 4–6). These results are mostly comparable with those obtained under whole-cell clamp conditions (Fig. 1C). In Fig. 4, the potency of diCl-DHAA to activate BKα was compared with that of abietic acid and dehydroabietic acid, an aromatic derivative of abietic acid. The data for pimaric acid, a potent BK channel opener, were also taken from a previous study, where the potency of pimaric acid was determined under the same experimental conditions (Imaizumi et al., 2002). Even a high concentration of abietic acid at 30 and 100 μM failed to increase the activity of BKα, whereas dehydroabietic acid at 3 and 10 μM increased activity significantly. Nevertheless, diCl-DHAA was much more potent as an activator of BKα than dehydroabietic acid and pimaric acid.

Effects of diCl-DHAA on Characteristics of Single BKα Channel Currents. In Fig. 5, effects of diCl-DHAA on characteristics of single BKα channel currents were systematically examined in the excised inside-out patch configuration. The bathing and pipette solution contained symmetrical 140 mM K^+. The pCa in the bathing solution was 7. The conductance of BKα, which was determined by slope of the regression line between 0 and +70 mV, was 224.8 ± 4.1 and 224.8 ± 4.3 pS in the absence and presence of 10 μM diCl-DHAA, respectively (n = 6; $p > 0.05$; Fig. 5B), indicating that diCl-DHAA did not affect BKα channel conductance. The inward rectification shown at high potentials (more than +80 mV) was consistent with that reported as voltage-dependent block of BK channel by Na^+ (Yellen, 1984) and was not affected by diCl-DHAA. Moreover, the P_o in the absence and presence of 10 μM diCl-DHAA was calculated and plotted against test potentials in Fig. 5C. Under these conditions, the increase in P_o was voltage-dependent in the range of +30 to +130 mV, and a set of data were well described by Boltzmann relationship:

$$P_o = (1 - C)/[1 + \exp\{(V_{1/2} - V_m)/S\}] \quad (1)$$

where $V_{1/2}$, V_m, S, and C is the voltage required for half-maximum activation, membrane potential, slope factor, and constant, respectively. Application of 10 μM diCl-DHAA neither changed S nor C (S, 10.5 ± 1.5 and 12.2 ± 1.3 mV; C, 0.15 ± 0.03 and 0.13 ± 0.02 in the absence and presence of diCl-DHAA, respectively; n = 5), whereas it significantly shifted $V_{1/2}$ to a more negative potential (110.7 ± 3.3 and 72.4 ± 5.7mV, respectively; n = 5; $p < 0.01$).

In Fig. 6, the effects of diCl-DHAA on Ca^{2+} sensitivity of BKα were examined at 0 mV in asymmetrical 5.9/140 mM K^+ conditions. When Ca^{2+} concentration in the bathing solution was elevated in a pCa range between 7.0 and 5.0, the P_o was increased in a concentration-dependent manner (Fig. 6, A and B). The relationship between Ca^{2+} concentration and the P_o of BKα was fitted by the following equation:

$$P_o = (1 - C)/1 + (K_d/[Ca^{2+}]_i)^m \quad (2)$$

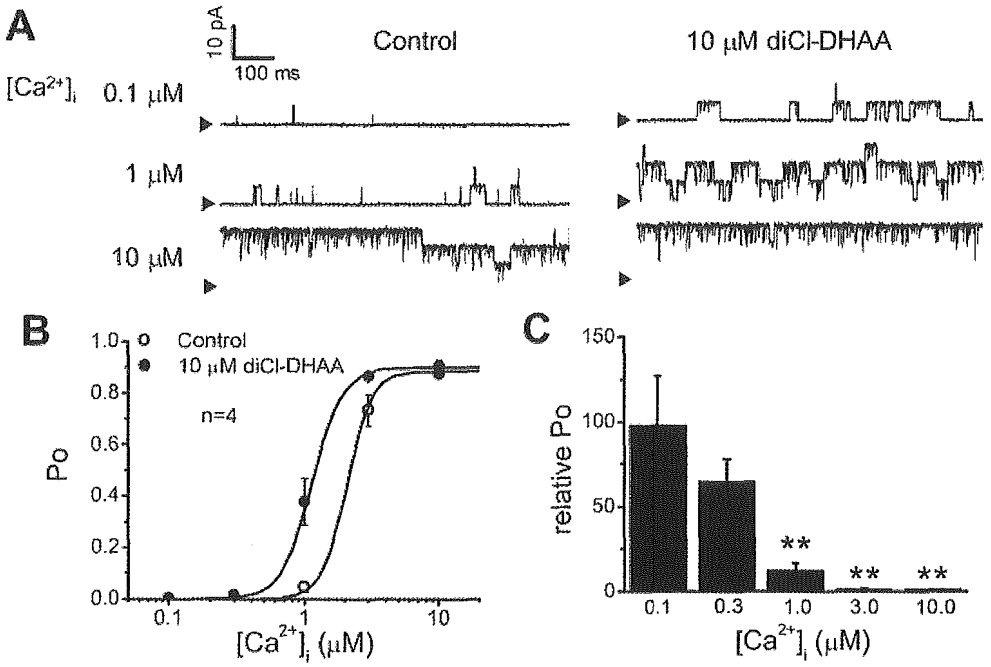

Fig. 6. Effects of diCl-DHAA on Ca^{2+} dependence of BKα. A, single channel currents of BKα were recorded in inside-out patch configuration at 0 mV in asymmetrical K^+ conditions (5.9/140 mM K^+) in the absence and presence of 10 μM diCl-DHAA. Recordings were obtained when $[Ca^{2+}]_i$ was 0.1, 1, or 10 μM. B, relationships between P_o and $[Ca^{2+}]_i$ were obtained in the absence (open circles) and presence of 10 μM diCl-DHAA (closed circles). Number of examples is four for each experiment. The data were fitted with the Hill equation (see *Results*). The fitted lines were plotted based on the following values of K_d, m, and C: 2.06, 4.65, and 0.15μM in the absence and 1.14, 3.83, and 0.10 μM in the presence of 10 μM diCl-DHAA, respectively. C, relative P_o in the presence of 10 μM diCl-DHAA versus that in the absence of 10 μM diCl-DHAA was re-evaluated at various $[Ca^{2+}]_i$ from the data shown in B. **, $p < 0.01$ versus relative P_o at 0.1 μM Ca^{2+}.

where K_d is an apparent dissociation constant of Ca^{2+}, $[Ca^{2+}]_i$ is the pCa in the bathing solution, m is a Hill coefficient, and C is a constant. Under the control conditions, K_d, m, and C, which were obtained from the best fitting, were pCa = 5.68 ± 0.03, 4.65 ± 0.92, and 0.152 ± 0.029, respectively (n = 4). In the presence of 10 μM diCl-DHAA, K_d was changed to pCa = 5.94 ± 0.03 (n = 4; $p < 0.05$), whereas the Hill coefficient, which indicates binding of one Ca^{2+} to each α subunit in the tetrameric complex of a functional BKα channel, was not significantly affected (3.83 ± 0.45; $p > 0.05$ versus control). C was 0.102 ± 0.008 and not affected by diCl-DHAA ($p > 0.05$ versus control). The relative P_o in the presence of 10 μM diCl-DHAA to that of the control was plotted against $[Ca^{2+}]_i$ in Fig. 6C. The lower the P_o in the control conditions, the larger the enhancement by diCl-DHAA.

Effects of diCl-DHAA on the kinetic properties of BKα were examined in excised inside-out patches, which included only one channel (Fig. 7). These patches had a single channel event even when $[Ca^{2+}]_i$ was elevated to pCa = 3.5. Figure 7A shows original current traces of BKα at pCa = 6.5 in the absence and presence of 10 μM diCl-DHAA. The data for open and closed dwell time in Fig. 7A were reconstituted as distribution histograms in Fig. 7, B and C, respectively. These histograms were well fitted by a double and triple exponential function, respectively (Fig. 7, B and C). As shown in Table 1, application of 10 μM diCl-DHAA caused a marked decrease in the mean closed time (τ_{Cs}) and its relative magnitude (A_{Cs}) of the slow component (4–5 times change), whereas other parameters were moderately changed (τ_{Os}, τ_{Cf}, τ_{Ci}, and A_{Of}) or were not affected (τ_{Of}, A_{Os}, A_{Cf}, and A_{Ci}) (n = 5).

Comparison of diCl-DHAA-Induced Effects on BKα with Those on BK$\alpha\beta$1. The enhancement of single BKα channel activity by diCl-DHAA indicated the direct action of this compound on BKα. It has been, however, established that coexpression of β1 subunit with BKα increases the sensitivity of BKα to Ca^{2+} and voltage (Wallner et al., 1996; Cox

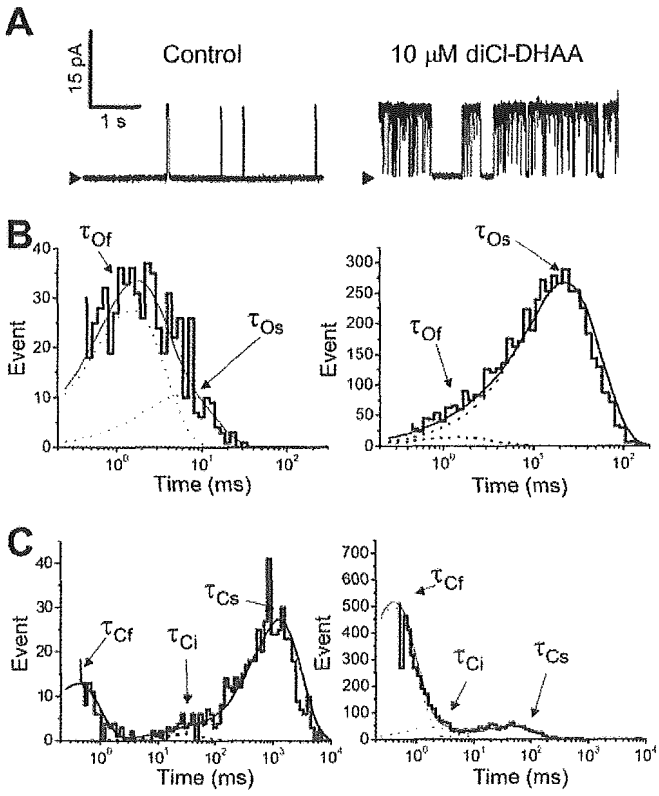

Fig. 7. Kinetics of diCl-DHAA-induced activation of BKα. A, single channel currents of BKα were recorded at +50 mV in inside-out patch configuration at pCa = 6.5 in symmetrical 140 mM K^+ conditions. B, dwell-time histograms of open times before (left) and after (right) application of 10 μM diCl-DHAA. The open-time histogram in the absence and presence of diCl-DHAA was fitted by a double exponential function. τ_{Of} and τ_{Os} represent time constants of the fast and slow components of the open times in BKα kinetics, respectively. Continuous lines show the sum of individual components (dotted lines). C, dwell-time histograms of closed times before (left) and after (right) application of 10 μM diCl-DHAA. The closed time histogram was fitted by a triple exponential function. τ_{Cf}, τ_{Ci}, and τ_{Cs} represent time constants of the fast, intermediate, and slow components of closed times, respectively.

and Aldrich, 2000). To determine whether diCl-DHAA also acts on the functional coupling between BKα and β1 subunits, the increase in P_o by diCl-DHAA in BK$\alpha\beta$1 was compared with that in BKα in inside-out patches. The P_o of BKα at pCa = 7.0 was increased at any test potential by coexpression with β1 subunit (Fig. 8A). Since the increase in P_o by diCl-DHAA depended on a basal P_o before application (Fig. 6C), effects of diCl-DHAA on BKα at +40 mV were compared with those on BK$\alpha\beta$1 at +20 mV. The basal P_o values were comparable with each other (0.0028 ± 0.0006 versus 0.0023 ± 0.0006; n = 5; Fig. 8B). The application of 1 μM diCl-DHAA increased the P_o to 0.0180 ± 0.0058 in BKα (n = 5; $p < 0.05$) and to 0.0208 ± 0.0037 in BK$\alpha\beta$1 (n = 5; $p < 0.01$). The ratio of P_o in BKα in the presence and absence of diCl-DHAA was 7.2 ± 0.8 and therefore not significantly different from that in BK$\alpha\beta$1 (11.1 ± 3.1; $p > 0.05$). This finding strongly suggests that coexpression of β1 subunit did not affect the diCl-DHAA-induced enhancement of BKα.

Selectivity of diCl-DHAA on BK Channel Versus Voltage-Dependent Ca^{2+} Channel. To examine whether the action of diCl-DHAA is selective to BK channels over CaV channels, effects of 0.3 and 1 μM diCl-DHAA on BKα were compared with those on CaV channel currents in HEK293 cells, which coexpressed α1 subunit of rabbit CaV channel and β3 subunit of mouse CaVα1Cβ3. Here, effects of pimaric acid on CaVα1Cβ3 were also examined. The inward currents through CaVα1Cβ3 were elicited upon depolarization from a holding potential of −60 mV to test potentials in a range of −50 and +40 mV by 10-mV step every 10 s. The maximum amplitude was obtained at +10 mV (peak amplitude, 193 ± 54.4 pA; n = 6; Fig. 9A). CaVα1Cβ3 channel currents were not inhibited by 0.3 μM diCl-DHAA or pimaric acid, whereas they were significantly inhibited by both compounds at 1 μM (only diCl-DHAA; Fig. 9A). Data about effects of diCl-DHAA and pimaric acid on BKα are those shown in Fig. 3 and provided in a previous study (Imaizumi et al., 2002) and were obtained in inside-out patches at +40 mV and pCa = 7.0 under symmetrical 140 mM K^+ conditions. Enhancement of BK channel activity by diCl-DHAA was significant at 0.3 and 1 μM, indicating that 0.3 μM diCl-DHAA is selective for the BK channel over the CaV channel.

TABLE 1
Time constants and relative weights

	Control	diCl-DHAA	diCl-DHAA/ Control
Time constants (ms)			
τ_{Of}	1.49 ± 0.17	1.53 ± 0.22	1.02 ± 0.10
τ_{Os}	10.34 ± 3.75	23.73 ± 5.38	2.68 ± 0.52*
τ_{Cf}	0.65 ± 0.05	0.74 ± 0.04	1.14 ± 0.04*
τ_{Ci}	43.32 ± 11.05	11.33 ± 3.96	0.41 ± 0.16*
τ_{Cs}	1955.19 ± 560.17	264.08 ± 77.97	0.21 ± 0.07**
Relative weights			
A_{Of}	0.53 ± 0.11	0.16 ± 0.04	0.40 ± 0.12**
A_{Os}	0.47 ± 0.11	0.84 ± 0.04	2.15 ± 0.44
A_{Cf}	0.40 ± 0.08	0.82 ± 0.02	2.43 ± 0.54
A_{Ci}	0.12 ± 0.04	0.11 ± 0.01	1.74 ± 0.73
A_{Cs}	0.44 ± 0.11	0.07 ± 0.02	0.23 ± 0.07**

*$p < 0.05$ and **$p < 0.01$ vs. unity (n = 5).

Discussion

In the present study, we have demonstrated that diCl-DHAA is one of the most potent synthesized activators affecting the BKα subunit via changing the voltage and Ca^{2+} sensitivity of the channel. Chemical modification of abietic acid, an inactive compound, to dehydroabietic acid and diCl-DHAA provides a potent and selective BK channel opener. The latter has an inverse voltage dependence for BKα channel activation and is one of the most potent openers available by application from outside of the cell membrane.

BK channels consist of channel-forming α subunits and accessory β subunits (β1–β4) arranged in tetramers (Vergara et al., 1998). Each β subunit interacts with N-terminal region of an α subunit (Wallner et al., 1996) and regulates the activity of the α subunit by changing Ca^{2+} and voltage sensitivity and/or channel kinetics. Although only one major type of α subunit with splice variants has been defined, the combination of the BK channel α subunit encoded by KCNMA1 and β subunits encoded by KCNMB1-4 provides the

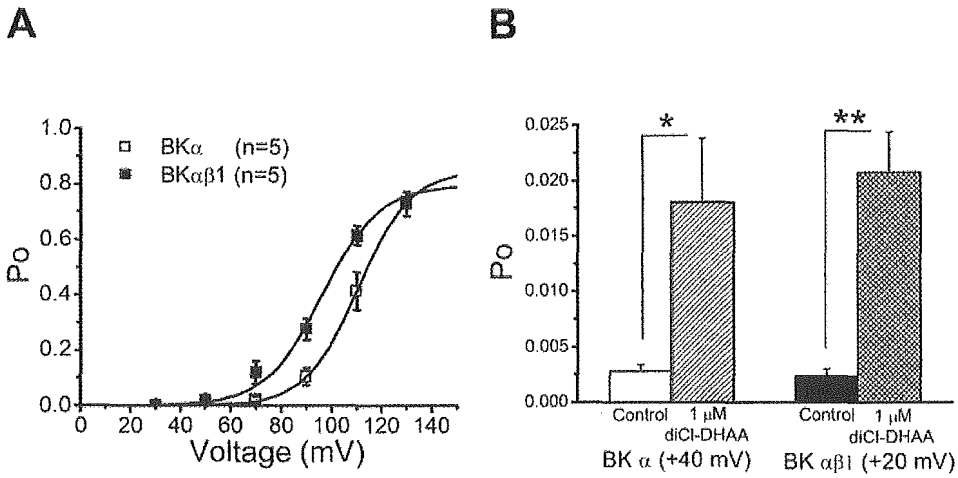

Fig. 8. Comparison of effects of diCl-DHAA on single channel currents due to BKα or BK$\alpha\beta$1. A, relationships between P_o and test potentials were obtained in HEKBKα (open squares) and HEKBK$\alpha\beta$1 (closed squares). Recordings were obtained at pCa = 7.0 in symmetrical 140 mM K^+ conditions. Number of examples is five for each experiment. The data were fitted using the Boltzmann equation (see *Results*). The fitted lines are based on the following values of $V_{1/2}$, S, and C: 110.7 mV, 10.5 mV, and 0.15 in HEKBKα and 96.3 mV, 11.4 mV, and 0.20 in HEKBK$\alpha\beta$1, respectively. B, effect of 1 μM diCl-DHAA on P_o of BK$\alpha\beta$1 was compared with that of BKα. The P_o of BKα in the absence of diCl-DHAA was 0.00382 ± 0.00104 at +40 mV and close to P_o of BK$\alpha\beta$1 at +20 mV (0.00346 ± 0.00079; $p > 0.05$). Number of examples is five for each. *, $p < 0.05$ and **, $p < 0.01$ versus the corresponding control.

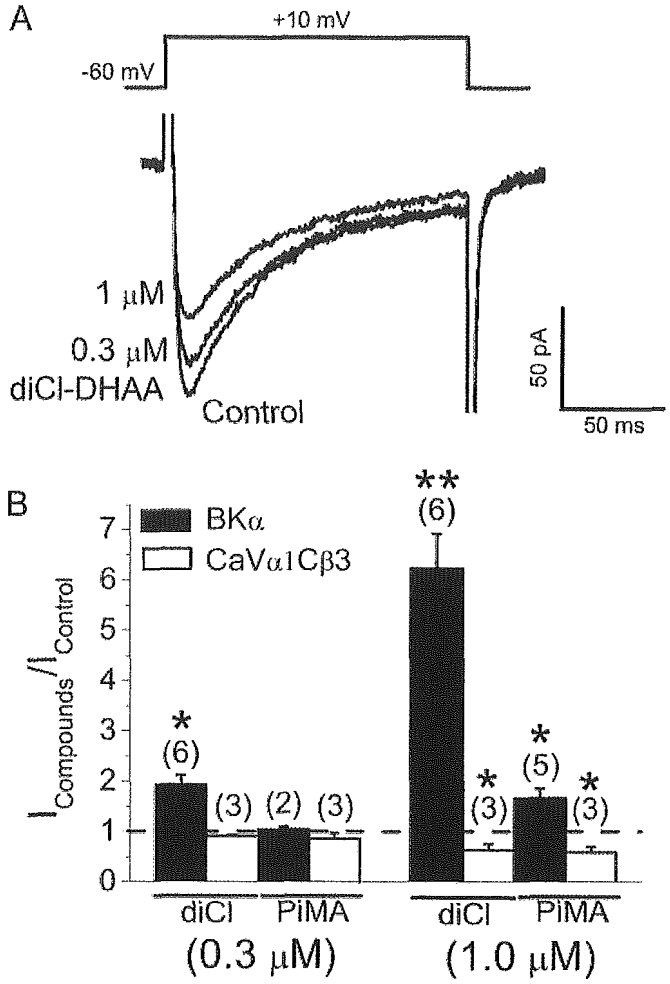

Fig. 9. Inhibitory effects of diCl-DHAA and pimaric acid on CaV channel currents. A, representative current traces obtained from HEKs coexpressing rabbit α1C and mouse β3 with GFP (see *Materials and Methods*). The inward currents were elicited by 150-ms depolarizing pulses to +10 mV from a holding potential of −60 mV in the absence and presence of 0.3 or 1 μM diCl-DHAA. B, summary of effects of diCl-DHAA and pimaric acid on CaV channel currents (closed columns). For comparison, their effects on BKα are also illustrated. Inhibitory effects of diCl-DHAA and pimaric acid on CaV channel currents were examined in experiments identical to that shown in A, and the relative amplitude of inward currents at +10 mV in the presence of each compound was determined taking the amplitude in the absence as unity. For revaluation of effects of diCl-DHAA and pimaric acid on BKα, the same set of data shown in Fig. 3 (present study) and Fig. 5 (Imaizumi et al., 2002) were used. Means ± S.E.M. are shown by columns and vertical bars, respectively. The number in parenthesis denotes number of cells used. *, $p < 0.05$ and **, $p < 0.01$ versus unity.

diversity of BK channels (McManus et al., 1995; Brenner et al., 2000a; Uebele et al., 2000), which offers opportunities of development of new therapeutic agents. Benzimidazolone derivatives such as biarylureas (NS-1608), NS-1619, BMS-204352 (Gribkoff et al., 2001), arylpyrrole (NS-8), and indole-3-carboxylic acid esters (CGS-7181 and CGS-7184) have been characterized as effective BK channel openers (Coghlan et al., 2001).

Natural products have also been evaluated as BK channel openers, and terpenoids such as dehydrosoyasaponin I (McManus et al., 1993), maxikdiol (Singh et al., 1994), and L-735,334 (Lee et al., 1995) have been identified as active BK channel openers. Our pioneer work of pimarane compounds, which have a close structural similarity to maxikdiol, has revealed that pimaric acid is a potent BK channel opener that interacts with BKα subunit but not with the BKβ1 subunit (Imaizumi et al., 2002). Pimaric acid activates BK channels in HEKBK$\alpha\beta$1 when applied externally as well as when applied to the "internal phase" in inside-out patches. Its potency seems to be slightly higher than that of maxikdiol. An important comparative result in the previous study is that abietic acid did not show BK channel opening action despite of the fact that abietic acid is a structural isomer ($C_{20}H_{30}O_2$) of pimaric acid.

Of importance is our recent finding that chemical modification of abietic acid to dehydroabietic acid as well as diCl-DHAA produced compounds active to the open BK channel (Ohwada et al., 2003). In the present study, we provided new information about mechanisms of diCl-DHAA-induced activation of BK channels. diCl-DHAA activated BK channels in HEKBKα when applied externally as well as when applied to the internal phase in inside-out patches. Its potency was obviously higher than that of pimaric acid in whole-cell recording under the same experimental conditions, since significant activation was observed at 0.1 μM diCl-DHAA (Imaizumi et al., 2002). Dehydrosoyasaponin-I (Giangiacomo et al., 1998), 17β-estradiol (Valverde et al., 1999), and tamoxifen (Dick et al., 2001) interact with β subunits of BK channels to increase the channel activity. In contrast, NS-1619 (Ahring et al., 1997), epoxyeicosatrienoic acid (Fukao et al., 2001), Evans blue (Yamada et al., 2001), and pimaric acid (Imaizumi et al., 2002) act on the BKα subunit. Our results clearly showed that diCl-DHAA interacts with the BKα subunit but may not interact with the BKβ1 subunit. We also found that 100 nM iberiotoxin completely removed the diCl-DHAA-induced potentiation of the macroscopic BK$\alpha\beta$1 channel currents. This finding suggests that diCl-DHAA does not affect the iberiotoxin binding to BK$\alpha\beta$1, although effects of diCl-DHAA on ^{125}I-iberiotoxin binding were not examined in this study. Consistently, the concentration-response relationship of charybdtoxin for the inhibition of macroscopic BK$\alpha\beta$1 channel currents was not affected by the presence of 10 μM pimaric acid, which has a close structural analogy to diCl-DHAA (Imaizumi et al., 2002).

It is obvious from the present results that diCl-DHAA activates BK channels in a voltage- and Ca^{2+}-dependent manner. It is very notable that the potentiation of BK channel activity by diCl-DHAA was significantly larger at negative potentials as well as at lower Ca^{2+} concentrations. In contrast, BMS-204352, a potent BK channel opener, caused activation of BK channel currents only at positive potentials (more than +30 mV; Gribkoff et al., 2001; Schrøder et al., 2003). To our knowledge, diCl-DHAA, and presumably pimaric acid as well, are the only compounds that show marked inversed voltage dependence for potentiation among various types of BK channel openers. This characteristic feature of diCl-DHAA can be considered particularly effective to prevent membrane depolarization, hyperexcitability, and/or excess Ca^{2+} influx to the cell and may be advantageous for clinical use. Moreover, diCl-DHAA decreased the time for the channels to stay in the prolonged closed states. It can be, therefore, suggested that this kinetic change in the presence of diCl-DHAA causes activation of BK channel. Niflumic acid opens BK channels mainly by decreasing the time in the long-closed states (Ottolia and Toro, 1994).

It is important to characterize the selectivity of diCl-DHAA to BK channels over that of other ion channels. We found that diCl-DHAA at concentrations of 0.3 μM or less increased BK channel activity without inhibiting CaV channels. Moreover, even though diCl-DHAA-induced inhibition of CaV channels at 1 μM was comparable with that by 1 μM pimaric acid (~30% of the control), the activation of BK channel currents by diCl-DHAA was significantly greater than that by pimaric acid, suggesting that the potent activation of BK channels by diCl-DHAA provides more selectivity against CaV channels than that by pimaric acid. The selectivity of BK channel openers against CaV channels has not been well defined, but nordihydroguaiaretic acid or NS-1619-induced inhibition of CaV channel currents was comparable with or slightly more potent than the activation of BK channels, respectively (Holland et al., 1996; Yamamura et al., 1999). For development of potent and selective BK channel openers, scaffoldings of dehydroabietic acid may be useful (Ohwada et al., 2003).

Effects of diCl-DHAA on small (SK) and intermediate (IK) conductance Ca^{2+}-activated K^+ channels were not examined systematically in this study. BK channel openers reported so far, including pimaric acid, are however selective over SK and IK channels (Kaczorowski and Garcia, 1999; Coghlan et al., 2001; Imaizumi et al., 2002), and our preliminary data suggest that 1 μM diCl-DHAA did not affect the activities of SK2 and SK4 channels (K. Sakamoto, unpublished data). Genetically, and even functionally in some aspects, KCNMA (BK) is closer to voltage-dependent K^+ channels than KCNN (SK and IK), because of the presence of its voltage-sensitive domain (Vergara et al., 1998). It is therefore worth examining the effects of diCl-DHAA on cloned voltage-dependent K^+ channels, which remain to be determined.

In conclusion, our results provide new information of mechanisms underlying diCl-DHAA-induced activation of BK channels and the selectivity against CaV channels. diCl-DHAA is effective from either side of cell membrane and acts on BKα subunit to increase Ca^{2+} and voltage sensitivity. In contrast to many other BK channel openers, the effect of diCl-DHAA on BKα significantly showed inverse voltage dependence, i.e., larger potentiation at lower membrane potentials. In this respect, diCl-DHAA may be one of the most potent BK channel openers ever known to sensitize the negative feedback control of $[Ca^{2+}]_i$ regulation via activation of BK channels, which suppress depolarization from resting membrane potential, and subsequently, membrane excitability. diCl-DHAA at low concentrations (<1 μM) shows selectivity to the BK channel over CaV channels and possesses higher selectivity to BK channels than pimaric acid. Dehydroabietic acid, including diCl-DHAA, is a new prototype scaffolding as a potent BKα channel opener.

Acknowledgments

We thank Dr. Wayne Giles (University of Calgary, Calgary, AB, Canada) for providing data acquisition and analysis programs for macroscopic current analyses and also for critical reading of this manuscript. We also thank Dr. John Dempster (University of Strathclyde) for providing data acquisition and analysis programs for single channel analyses.

References

Ahring PK, Strobaek D, Christophersen P, Olesen SP, and Johansen TE (1997) Stable expression of the human large-conductance Ca^{2+}-activated K^+ channel α- and β-subunits in HEK293 cells. *FEBS Lett* **415:**67–70.

Bolton TB and Imaizumi Y (1996) Spontaneous transient outward currents in smooth muscle cells. *Cell Calcium* **20:**141–152.

Brenner R, Jegla TJ, Wickenden A, Liu Y, and Aldrich RW (2000a) Cloning and functional characterization of novel large conductance calcium-activated potassium channel β subunits, hKCNMB3 and hKCNMB4. *J Biol Chem* **275:**6453–6461.

Brenner R, Perez GJ, Bonev AD, Eckman DM, Kosek JC, Wiler SW, Patterson AJ, Nelson MT, and Aldrich RW (2000b) Vasoregulation by the β1 subunit of the calcium-activated potassium channel. *Nature (Lond)* **407:**870–876.

Coghlan MJ, Carroll WA, and Gopalakrishnan M (2001) Recent developments in the biology and medicinal chemistry of potassium channel modulators: update from a decade of progress. *J Med Chem* **44:**1627–1653.

Cox DH and Aldrich RW (2000) Role of the beta1 subunit in large-conductance Ca(2+)-activated K(+) channel gating energetics. Mechanisms of enhanced Ca(2+) sensitivity. *J Gen Physiol* **116:**411–432.

Dick GM, Rossow CF, Smirnov S, Horowitz B, and Sanders KM (2001) Tamoxifen activates smooth muscle BK channels through the regulatory β1 subunit. *J Biol Chem* **276:**34594–34599.

Fernández-Fernández JM, Tomas M, Vazquez E, Orio P, Latorre R, Senti M, Marrugat J, and Valverde MA (2004) Gain-of-function mutation in the KCNMB1 potassium channel subunit is associated with low prevalence of diastolic hypertension. *J Clin Investig* **113:**1032–1039.

Fukao M, Mason HS, Kenyon JL, Horowitz B, and Keef KD (2001) Regulation of BKCa channels expressed in human embryonic kidney 293 cells by epoxyeicosatrienoic acid. *Mol Pharmacol* **59:**16–23.

Giangiacomo KM, Kamassah A, Harris G, and McManus OB (1998) Mechanism of maxi-K channel activation by dehydrosoyasaponin-I. *J Gen Physiol* **112:**485–501.

Gribkoff VK, Starrett JE Jr, Dworetzky SI, Hewawasam P, Boissard CG, Cook DA, Frantz SW, Heman K, Hibbard JR, Huston K, et al. (2001) Targeting acute ischemic stroke with a calcium-sensitive opener of maxi-K potassium channels. *Nat Med* **7:**471–477.

Holland M, Langton PD, Standen NB, and Boyle JP (1996) Effects of the BK_{Ca} channel activator, NS1619, on rat cerebral artery smooth muscle. *Br J Pharmacol* **117:**119–129.

Imaizumi Y, Muraki K, and Watanabe M (1989) Ionic currents in single smooth muscle cells from the ureter of the guinea-pig. *J Physiol (Lond)* **411:**131–159.

Imaizumi Y, Ohi Y, Yamamura H, Ohya S, Muraki K, and Watanabe M (1999) Ca^{2+} spark as a regulator of ion channel activity. *Jpn J Pharmacol* **80:**1–8.

Imaizumi Y, Sakamoto K, Yamada A, Hotta A, Ohya S, Muraki K, Uchiyama M, and Ohwada T (2002) Molecular basis of pimarane compounds as novel activators of large-conductance Ca^{2+}-activated K^+ channel α-subunit. *Mol Pharmacol* **62:**836–846.

Imaizumi Y, Torii Y, Ohi Y, Nagano N, Atsuki K, Yamamura H, Muraki K, Watanabe M, and Bolton TB (1998) Ca^{2+} images and K^+ current during depolarization in smooth muscle cells of the guinea-pig vas deferens and urinary bladder. *J Physiol (Lond)* **510:**705–719.

Kaczorowski GJ and Garcia ML (1999) Pharmacology of voltage-gated and calcium-activated potassium channels. *Curr Opin Chem Biol* **3:**448–458.

Lawson K (2000) Potassium channel openers as potential therapeutic weapons in ion channel disease. *Kidney Int* **57:**838–845.

Lee SH, Hensens OD, Helms GL, Liesch JM, Zink DL, Giacobbe RA, Bills GF, Stevens-Miles S, Garcia ML, and Schmalhofer WA (1995) L-735,334, a novel sesquiterpenoid potassium channel-agonist from *Trichoderma virens*. *J Nat Prod* **58:**1822–1828.

McManus OB, Harris GH, Giangiacomo KM, Feigebaum P, Reuben JP, Addy ME, Burka JF, Kaczorowski GJ, and Garcia ML (1993) An activator of calcium-dependent potassium channels isolated from a medicinal herb. *Biochemistry* **32:**6128–6133.

McManus OB, Helms LM, Pallanck L, Ganetzky B, Swanson R, and Leonard RJ (1995) Functional role of the beta subunit of high conductance calcium-activated potassium channels. *Neuron* **14:**645–650.

Murakami M, Yamamura H, Suzuki T, Kang M, Ohya S, Murakami A, Miyoshi I, Sasano H, Muraki K, Hano T, et al. (2003) Modified cardiovascular L-type channels in mice lacking the voltage-dependent Ca^{2+} channel β3 subunit. *J Biol Chem* **278:**43261–43267.

Nelson MT and Quayle JM (1995) Physiological roles and properties of potassium channels in arterial smooth muscle. *Am J Physiol* **268:**C799–C822.

Ohi Y, Yamamura H, Nagano N, Ohya S, Muraki K, Watanabe M, and Imaizumi Y (2001) Local Ca^{2+} transients and distribution of BK channels and ryanodine receptors in smooth muscle cells of guinea-pig vas deferens and urinary bladder. *J Physiol (Lond)* **534:**313–326.

Ohwada T, Nonomura T, Maki K, Sakamoto K, Ohya S, Muraki K, and Imaizumi Y (2003) Dehydroabietic acid derivatives as a novel scaffold for large-conductance calcium-activated K^+ channel openers. *Bioorg Med Chem Lett* **13:**3971–3974.

Ottolia M and Toro L (1994) Potentiation of large conductance K_{Ca} channels by niflumic, flufenamic and mefenamic acids. *Biophys J* **67:**2272–2279.

Schrøder RL, Strobaek D, Olesen SP, and Christophersen P (2003) Voltage-independent KCNQ4 currents induced by (±)BMS-204352. *Pflueg Arch Eur J Physiol* **446:**607–616.

Singh SB, Goetz MA, Zink DL, Dombrowski AW, Polishook JD, Garcia ML, Schmalhofer W, McManus OB, and Kaczorowski GJ (1994) Maxikdiol: a novel dihydroxyisoprimane as an agonist of maxi-K channels. *J Chem Soc Perkin Trans* **1:**3349–3352.

Uebele VN, Lagrutta A, Wade T, Figueroa DJ, Liu Y, McKenna E, Austin CP, Bennett PB, and Swanson R (2000) Cloning and functional expression of two families of beta-subunits of the large conductance calcium-activated K^+ channel. *J Biol Chem* **275:**23211–23218.

Valverde MA, Rojas P, Amigo J, Cosmelli D, Orio P, Bahamonde MI, Mann GE, Vergara C, and Latorre R (1999) Acute activation of maxi-K channels (hSlo) by estradiol binding to the β subunit. *Science (Wash DC)* **285:**1929–1931.

Vergara C, Latorre R, Marrion NV, and Adelman JP (1998) Calcium-activated potassium channels. *Curr Opin Neurobiol* **8:**321–329.

Wallner M, Meera P, and Toro L (1996) Determinant for β-subunit regulation in high-conductance voltage-activated and Ca^{2+}-sensitive K^+ channels: an additional transmembrane region at the N terminus. *Proc Natl Acad Sci USA* **93:**14922–14927.

Wellman GC and Nelson MT (2003) Signaling between SR and plasmalemma in smooth muscle: sparks and the activation of Ca^{2+} sensitive ion channels. *Cell Calcium* **34:**211–229.

Yamada A, Gaja N, Ohya S, Muraki K, Narita H, Ohwada T, and Imaizumi Y (2001) Usefulness and limitation of $DiBAC_4(3)$, a voltage-sensitive fluorescent dye, for the measurement of membrane potentials regulated by recombinant large conductance Ca^{2+}-activated K^+ channels in HEK293 cells. *Jpn J Pharmacol* **86:**342–350.

Yamamura H, Nagano N, Hirano M, Muraki K, Watanabe M, and Imaizumi Y (1999) Activation of Ca^{2+}-dependent K^+ current by nordihydroguaiaretic acid in porcine coronary arterial smooth muscle cells. *J Pharmacol Exp Ther* **291:** 140–146.

Yellen G (1984) Ionic permeation and blockade in Ca^{2+}-activated K^+ channels of bovine chromaffin cells. *J Gen Physiol* **84:**157–186.

Address correspondence to: Dr. Yuji Imaizumi, Department of Molecular and Cellular Pharmacology, Graduate School of Pharmaceutical Sciences, Nagoya City University, 3-1 Tanabedori, Mizuhoku, Nagoya 467-8603, Japan. E-mail: yimaizum@phar.nagoya-cu.ac.jp

Available online at www.sciencedirect.com

SCIENCE DIRECT®

European Journal of Pharmacology 518 (2005) 107 – 110

www.elsevier.com/locate/ejphar

Short communication

Purification and aqueous phase atomic force microscopic observation of recombinant $P2X_2$ receptor

Ken Nakazawa [a,*], Yoko Yamakoshi [b,1], Toshie Tsuchiya [c], Yasuo Ohno [a]

[a] *Division of Pharmacology, National Institute of Health Sciences, 1-18-1 Kamiyoga, Setagaya, Tokyo 158-8501, Japan*
[b] *Division of Organic Chemistry, National Institute of Health Sciences, 1-18-1 Kamiyoga, Setagaya, Tokyo 158-8501, Japan*
[c] *Division of Medical Devices, National Institute of Health Sciences, 1-18-1 Kamiyoga, Setagaya, Tokyo 158-8501, Japan*

Received 4 April 2005; received in revised form 14 June 2005; accepted 20 June 2005
Available online 28 July 2005

Abstract

Recombinant $P2X_2$ receptor was observed by atomic force microscope in the aqueous phase. The $P2X_2$ receptor was expressed in an insect cell line, and recombinant proteins were prepared under native conditions. The membrane fractions were extracted, and histidine-tagged receptor protein was purified from the fractions by column chromatography. When the purified protein fraction was diluted with water and served for atomic force microscopy, dispersed particles of about 3 nm in height were observed. In the presence of 1 mM ATP, the assembly-like images of the particles were obtained. More densely assembled images of the particles were achieved when the protein was dissolved in a Tris buffer containing 1 mM ATP. Under this condition, imaging of the surface of the particles exhibited a circular structure with a diameter of about 10 nm having a pore-like structure. These results suggest that atomic force microscopy provides structural information about $P2X_2$ receptor in aqueous phase.

Keywords: P2X receptor; Atomic force microscopy; Protein structure; ATP

1. Introduction

P2X receptors are ion channel forming membrane proteins that are activated by extracellular ATP, and their physiological roles have been shown in various tissues including the central nervous system (see reviews, Khakh, 2001; North, 2002; Vial et al., 2004). This ion channel/receptor family consists of 7 subclasses ($P2X_1$ to $P2X_7$), and is believed to have molecular structures distinct from so-called "ligand-gated channel super family" including nicotinic acetylcholine receptor/channels and ionotropic glutamate receptor channels. Structural analyses such as the X-ray crystal analysis have not been made for P2X receptor/channel family. In addition, because of their distinct structures, estimation from homology modeling based on known three-dimensional structures of other proteins is difficult. Thus, information concerning the structure and morphology of P2X receptor is lacking. Atomic force microscopy is an approach for structural analysis that allows the analysis of a small amount (nanogram to microgram) of uncrystalized protein. Atomic microscopy enables the observation of both individual and assembled protein molecules in the aqueous phase, which may reveal dynamic forms of biologically active proteins (Müller and Engel, 2002). Recently, Barrera et al. (2005) reported atomic force microscopy imaging of dried P2X receptor protein. In the present study, we have prepared $P2X_2$ receptor protein from an insect cell line expression system, and made atomic force microscopy imaging in aqueous phase. The imaging has revealed that $P2X_2$ receptor is a pore-forming protein for the first time.

* Corresponding author. Tel.: +81 3 3700 9704; fax: +81 3 3707 6950.
E-mail address: nakazawa@nihs.go.jp (K. Nakazawa).
[1] Present address: Center for Polymers and Organic Solids, Department of Chemistry and Biochemistry, University of California, Santa Barbara, CA 93106-9510, USA.

0014-2999/$ - see front matter © 2005 Elsevier B.V. All rights reserved.
doi:10.1016/j.ejphar.2005.06.018

2. Materials and methods

2.1. Preparation of recombinant $P2X_2$ receptor protein

N-terminal hexahistidine-tagged recombinant rat $P2X_2$ receptor was expressed using baculovirus-Sf9 system, which has been used for the expression of membrane receptor proteins (e.g., Boundy et al., 1993; Ng et al., 1993). cDNA encoding rat $P2X_2$ receptor (Brake et al., 1994) was subcloned into pFast BAC HTc vector (BD Bioscience Clonetech, Palo Alto, CA, USA). The recombinant virus was transfected to insect-derived clonal Sf9 cells. After culturing at a volume of 500 ml at room temperature, the culture medium was centrifuged at 130 $\times g$ for 5 min, and the precipitated cells were washed with Ca^{2+}, Mg^{2+}-free phosphate buffered saline (137 mM NaCl, 2.7 mM KCl, 8.1 mM Na_2HPO_4, and 1.5 mM KH_2PO_4; PBS(−)) twice. The cells were then suspended in a Tris–HCl (pH 7.4) lysis buffer containing Triton X-100, and homogenized. NaCl was added such that its final concentration became 100 mM. This solution was centrifuged at 30000 $\times g$ for 20 min, and the supernatant was then centrifuged at 380000 $\times g$ for 10 min. Polyacrylamide gel electrophoresis followed by immunoblotting analysis with anti-hexahistidine antibody showed that hexahistidine-tagged proteins of an expected size (56 kD) were found in this supernatant. Further purification was made using Chelating Sepharose FF colums. Ni^{2+}-bound columns were equilibrated with a buffer containing 20 mM Tris–HCl and 0.5 M NaCl (pH 8.0), and samples were applied. The bound receptor proteins were eluted by stepwise increase of imidazole (10, 20, 50, 100, 200 and 500 mM). The concentrations of the receptor protein in the eluted solutions were estimated by measuring absorbance at 595 nm. The most purified $P2X_2$ receptor protein (>90% of total protein) was found in the fraction eluted by 10 mM imidazole, and this fraction was served for atomic force microscopy imaging. The purified $P2X_2$ receptor exhibited the ability to bind ATP when photoaffinity labeling with [α-^{32}P]ATP was performed according to Kim et al. (1997). In this experiment, the binding of [α-^{32}P]ATP was markedly reduced by 100 μM nonradiolabeled ATP.

2.2. Atomic force microscopy imaging

The protein solution (about 1.5 μM) was diluted to appropriate concentrations (0.1 to 10 nM) with water, and the diluted solution was placed on freshly cleaved mica. After 30 min, unbound proteins were washed away with water, and served for atomic force microscopy imaging. When ATP (disodium salt; Sigma, St. Louis, MO, USA) was added to water, 1 mM solution was neutralized to pH 7.4 with 2 N NaOH (final Na^+ concentration was about 16 mM). In part of the experiments, the protein solution was diluted with a Tris buffer of the following composition (in millimolar): Tris 50, KCl 150, $MgCl_2$ 10, dithiothreirol 1 (pH 7.0). This buffer composition was similar to that utilized for atomic force microscopy imaging of *Escherichia coli* GroES (Cheung et al., 2000). Imaging was made in an aqueous tapping mode using MFP-3D (Asylum Research, Santa Barbara, CA, USA) equipped with OMCL-TR800PSA (Olympus, Tokyo, Japan) as a probe.

3. Results

Fig. 1A shows atomic force microscopy images of purified $P2X_2$ receptor proteins in water. A larger part of the proteins were found as dispersed particles. The height of single $P2X_2$ receptor proteins was about 3 nm (Fig. 1B). In the presence of 1 mM ATP, larger particles, presumably clots of several receptor proteins, were observed in addition to dispersed particles (Fig. 1C). A flatly and densely assembled image was obtained when the proteins were dissolved in a Tris buffer containing 1 mM ATP (Fig. 2A). Densely packed assembly is advantageous for atomic force microscopy imaging because resolution is improved due to smaller movement of probes along Z-axis (Müller and Engel, 2002). When the protein assembly shown in Fig. 2A was imaged at higher magnification, a circular structure with a pore was observed (Fig. 2B). The diameter of the circular structure was about 10 nm, and that of the pore was several nanometers. Without ATP, the protein was not densely assembled and did not exhibit uniform direction (not shown).

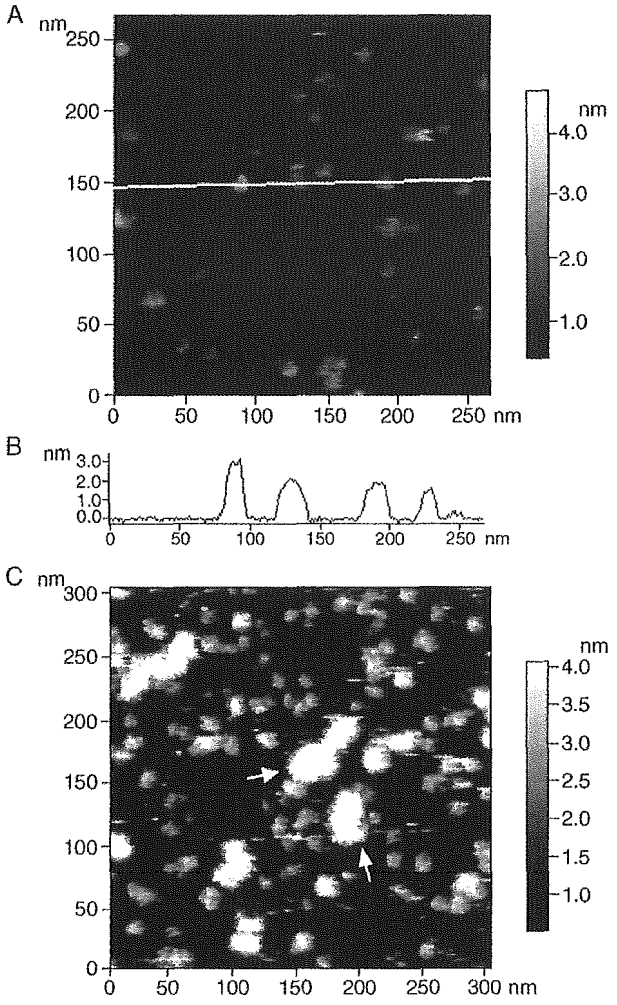

Fig. 1. (A) An atomic force microscopy image of $P2X_2$ receptor proteins in water. Isolated single receptor proteins and their small assemblies are seen. (B) A section of the image shown in (A). The section was made along with the line. The height of receptor proteins is about 3 nm or less. (C) An image of $P2X_2$ receptor proteins in the presence of 1 mM ATP. In addition to single receptor proteins, clots of the proteins (indicated by arrows) were also seen.

4. Discussion

For atomic force microscopy imaging of membrane proteins, densely expressed proteins in particular cells have

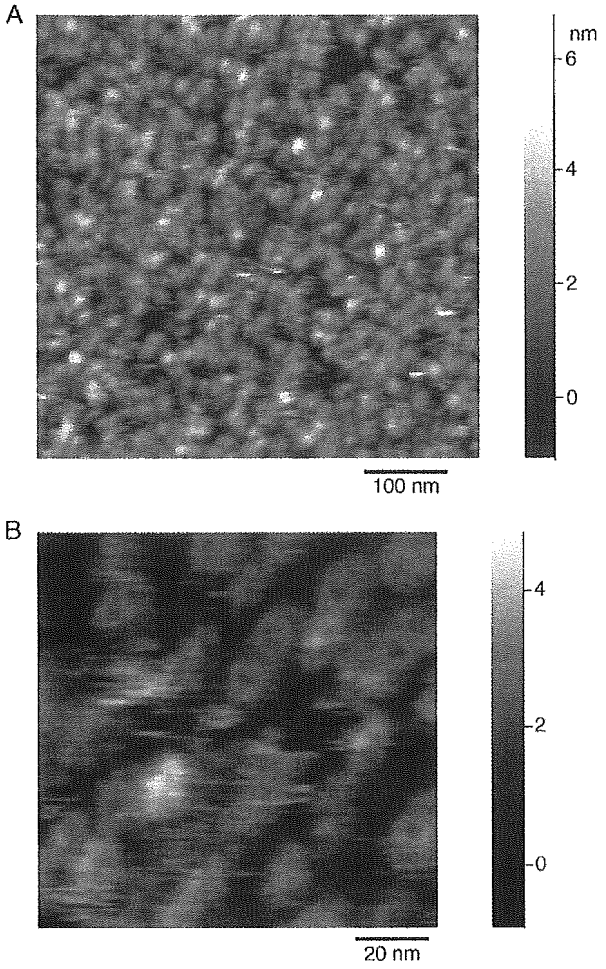

Fig. 2. (A) An image of $P2X_2$ receptor proteins in a Tris buffer containing 1 mM ATP. The proteins were flatly and densely assembled. (B) An expanded image. The upper surfaces of individual proteins exhibited a circular structure having a pore in its center.

been served in the presence of lipid bilayers (Müller and Engel, 2002; Müller et al., 2002). This two-dimensional (2D) protein crystal can provide high resolution of images, especially when combined with image processing including averaging. However, preparation of 2D crystals requires skilled techniques or special equipment. The present study has shown that recombinant $P2X_2$ can be imaged by atomic force microscopy without special techniques, but by simply adding agonist molecule, ATP. The role of ATP in promoting the densely packed assembly is unclear at present. It is speculated that receptor protein molecules without ATP freely move and exhibit various conformations, whereas ATP-bound receptor molecules exhibit only one or a restricted number of conformations in aqueous phase. The pore identified in the center of the protein may be the ion channel involved in $P2X_2$ receptor. A similar pore has been observed in connexin that also forms ion channels (Müller et al., 2002). It is unclear that the pore corresponds to the inner mouth or the outer mouth of the channel. Nevertheless, it is interesting that a number of proteins appear to exhibit similar surface structure (Fig. 2B). P2X receptor possesses a large extracellular domain, and, thus, it is possible that this domain is orientated upward to increase contact with the aqueous phase. Atomic force microscopy imaging of isolated membrane proteins may be less advantageous to elucidate biological functions compared to those embedded in lipid bilayer. However, isolated proteins are more readily observed than membrane preparations, and the imaging of these proteins may provide insights into the intrinsic properties of proteins and useful information to clarify the interactions between proteins and the membrane.

Barrera et al. (2005) observed dried $P2X_2$ receptor protein as a simple particle. We have revealed the outer structure of the protein, suggesting that resolution was better in the present study. However, our observation has not resolved trimeric assembly of $P2X_2$ receptor protein, which has been shown using antibodies specific for the protein (Barrera et al., 2005). Trimeric assembly of P2X receptor has been also demonstrated by electrophysiological and biochemical studies, and two transmembrane regions of each subunit are believed to contribute to the forming of channel pore (North, 2002; Vial et al., 2004). If $P2X_2$ receptor forms a six-barrel channel like connexin, this may account for a similar pore size (about several nanometers). Further improvement will be necessary to identify individual subunit proteins that form $P2X_2$ receptor and clarify more detailed structure by atomic force microscopy.

Acknowledgments

We are grateful to Dr. Jeffrey W. Bode of Department of Chemistry and Biochemistry, University of California, Santa Barbara for improving our manuscript. This work was partly supported by a Health and Labour Science Research Grant for Research on Advanced Medical Technology from the Ministry of Health, Labour and Welfare, Japan awarded to K.N., Y.Y. and T.T., and a grant-in-aid for scientific research from the Ministry of Education, Science, Sports and Culture, Japan (KAKENHI 13672319) awarded to K.N.

References

Barrera, N.P., Ormond, S.J., Henderson, R.M., Murrell-Langnado, R.D., Edwardson, J.M., 2005. AFM imaging demonstrates that $P2X_2$ receptors are trimers, but that $P2X_6$ receptor subunits do not oligomerize. J. Biol. Chem. 280, 10759–10765.

Boundy, V.A., Luedtke, R.R., Gallitano, A.L., Smith, J.E., Filtz, T.M., Kallen, R.G., Molinoff, P.B., 1993. Expression and characterization of the rat D3 dopamine receptor: properties and development of antibodies. J. Pharmacol. Exp. Ther. 264, 1002–1011.

Brake, A.J., Wagenbach, M.J., Julius, D., 1994. New structural motif for ligand-gated ion channels defined by an ionotropic ATP receptor. Nature 371, 519–523.

Cheung, C.L., Hafner, J.H., Lieber, C.M., 2000. Carbone nanotube atomic force microscopy tips: direct growth by chemical vapor deposition and application to high-resolution imaging. Proc. Natl. Acad. Sci., U. S. A. 97, 3809–3813.

Khakh, B.S., 2001. Molecular physiology of P2X receptors and ATP signalling at synapses. Nat. Rev. 2, 165–174.

Kim, M., Yoo, O.J., Choe, S., 1997. Molecular assembly of the extracellular domain of $P2X_2$, an ATP-gated ion channel. Biochem. Biophys. Res. Commun. 240, 618–622.

Müller, D.J., Engel, A., 2002. Conformations, flexibility, and interactions observed on individual membrane proteins by atomic force microscopy. Methods Cell Biol. 68, 257–298.

Müller, D.J., Hand, G.M., Engel, A., Sosinsky, G., 2002. Conformational changes in surface structures of isolated connexin 26 gap junctions. EMBO J. 21, 3598–3607.

Ng, G.Y., George, S.R., Zastawny, R.L., Caron, M., Bouvier, M., Dennis, M., O'Dowd, B.F., 1993. Human serotonin 1B receptor expression in Sf9 cells: phosphorylation, palmitoylation, and adenylyl cyclase inhibition. Biochemistry 32, 11727–11733.

North, R.A., 2002. Molecular physiology of P2X receptors. Physiol. Rev. 82, 1013–1067.

Vial, C., Roberts, J.A., Evans, R.J., 2004. Molecular properties of ATP-gated P2X receptor ion channels. Trends Pharmacol. Sci. 25, 487–493.

Available online at www.sciencedirect.com

SCIENCE DIRECT®

European Journal of Pharmacology 508 (2005) 23–30

www.elsevier.com/locate/ejphar

Characterization of voltage-dependent gating of $P2X_2$ receptor/channel

Ken Nakazawa[a,*], Yasuo Ohno[b]

[a]*Cellular and Molecular Pharmacology Section, Division of Pharmacology, National Institute of Health Sciences, 1-18-1 Kamiyoga, Setagaya, Tokyo 158-8501, Japan*

[b]*Division of Pharmacology, National Institute of Health Sciences, 1-18-1 Kamiyoga, Setagaya, Tokyo 158-8501, Japan*

Received 9 September 2004; received in revised form 29 November 2004; accepted 6 December 2004
Available online 4 January 2005

Abstract

The role of a voltage-dependent gate of recombinant $P2X_2$ receptor/channel was investigated in *Xenopus* oocytes. When a voltage step to −110 mV was applied from a holding potential of −50 mV, a gradual increase was observed in current evoked by 30 μM ATP. Contribution of this voltage-dependent component to total ATP-evoked current was greater when the current was evoked by lower concentrations of ATP. The voltage-dependent gate closed upon depolarization, and half the gates were closed at −80 mV. On the other hand, a potential at which half the gates opened was about −30 mV or more positive, which was determined using a series of hyperpolarization steps. The results of the present study suggest that the voltage-dependent gate behavior of $P2X_2$ receptor is not due to simple activation and deactivation of a single gate, but rather due to transition from a low to a high ATP affinity state.

Keywords: P2X receptor; Voltage dependence; Gate; Kinetics; Ligand affinity

1. Introduction

Extracellular ATP is considered a neurotransmitter, and its fast neurotransmission is mediated through ion channel-forming P2X receptors (see reviews, Ralevic and Burnstock, 1998; Khakh, 2001; North, 2002). To date, at least seven subclasses of P2X receptor ($P2X_{1-7}$) have been cloned, which form homo- or heteromeric receptors that act as functional ion channels (North and Surprenant, 2000). Each subclass consists of two transmembrane domains (TM1 and TM2) and one long extracellular domain (E1) between them. Both TM1 (Jiang et al., 2001; Haines et al., 2001) and TM2 (Rassendren et al., 1997; Egan et al., 1998; Migita et al., 2001) contribute to formation of the channel pore. P2X receptor/channels are permeable to cations, but demonstrate poor cation selectivity. The channels are gated by ATP molecules, and the narrowest part of the channel pore opens when activated (Rassendren et al., 1997). The ATP-binding site for gating is partly attributable to basic amino acid residues near the outer mouth of the channel pore formed by TM1 and TM2 (Ennion et al., 2000; Jiang et al., 2000), and the possibility that aromatic residues in E1 contribute to the binding site has also been suggested (Nakazawa et al., 2002; Roberts and Evans, 2004).

In addition to ATP, other factors are known to modulate channel activity. Zn^{2+} and acidic conditions facilitate ATP-mediated gating by increasing ATP sensitivity of $P2X_2$ receptor (Clyne et al., 2002). Neurotransmitters, including dopamine, and related compounds also facilitate ATP-mediated gating (Nakazawa et al., 1997a). Membrane potential may also play a role. It has been reported that ionic current activated by ATP is enhanced by hyperpolarization in pheochromocytoma PC12 cells (Nakazawa et al., 1997b). We observed similar voltage-dependent gating of recombinant $P2X_2$ receptor/channel, which was originally cloned from PC12 cells (Brake et al., 1994), and qualitatively analyzed its properties in the present study.

2. Methods

Recordings of ionic current through recombinant $P2X_2$ receptor/channels were performed according to our previous

* Corresponding author. Tel.: +81 3 3700 9704; fax: +81 3 3707 6950.
E-mail address: nakazawa@nihs.go.jp (K. Nakazawa).

0014-2999/$ - see front matter © 2004 Elsevier B.V. All rights reserved.
doi:10.1016/j.ejphar.2004.12.005

report (Nakazawa and Ohno, 1997). Briefly, the cloned rat $P2X_2$ receptor (Brake et al., 1994) was expressed in *Xenopus* oocytes by injecting in vitro transcribed cRNA. After 4 days of incubation at 18 °C, the membrane current of the oocytes was recorded. Oocytes were bathed in ND96 solution containing (in mM) NaCl 96, KCl 2, $CaCl_2$ 1.8, $MgCl_2$ 1, HEPES 5 (pH 7.5 with NaOH). In some experiments, oocytes were bathed in solution containing 10.8 mM $BaCl_2$ instead of 1.8 mM $CaCl_2$. When achieving a low extracellular chloride concentration, 96 mM Na-acetate was added instead of 96 mM NaCl. ATP (adenosine 5′-triphosphate disodium salt; Sigma, St. Louis, MO, U.S.A.) was applied by superfusion for approximately 10 s at regular 2-min intervals. Membrane current was recorded using the standard two-electrode voltage-clamp techniques, and electrical signals were stored on a data recorder (PC204Ax; SONY, Tokyo, Japan) for off-line analysis. Curve fittings to data were made using Microsoft' Excel X.

3. Results

3.1. Voltage-dependent component of ATP-evoked current

Fig. 1A compares membrane currents in the absence and presence of 30 μM ATP in a $P2X_2$ receptor-expressing oocyte. The oocyte was held at −50 mV and stepped to −110 mV for 200 ms. In the presence of ATP, inward current at −110 mV did not instantaneously reach steady-state, but gradually increased: a biphasic increase in current was observed with a voltage-independent component ("a" in Fig. 1A) and a voltage-dependent component ("b" in Fig. 1A). When the voltage was returned to −50 mV, a gradually declining inward "tail" current was observed ("c" in Fig. 1A). The voltage-dependent component of the inward current at −110 mV was observed to follow first-order kinetics with a time constant of 40 ms (Fig. 1B).

Fig. 2A demonstrates an increased magnitude of the voltage-dependent component when activated from a less negative holding potential. The voltage-dependent component was larger when the step to −110 mV was applied from −10 mV ("a" in Fig. 2A) than when it was applied from −70 mV ("b" in Fig. 2A). This dependence of the voltage-dependent component on holding potentials is illustrated in Fig. 2B. It is worth noting that Ca^{2+}-activated currents exist in *Xenopus* oocytes (Weber, 1999; Zhang and Hamill, 2000). Since P2X receptor/channels are Ca^{2+}-permeable (Khakh, 2001), a secondarily activated Ca^{2+}-induced current might contribute to the observed voltage-dependent changes. This does not, however, appear to be the case since a similar dependence on holding potentials was observed when extracellular Ca^{2+} was replaced with 10.8 mM Ba^{2+}. Time constants for the activation of the voltage-dependent component were obtained as shown in Fig. 1B, and the mean values were plotted against holding potentials

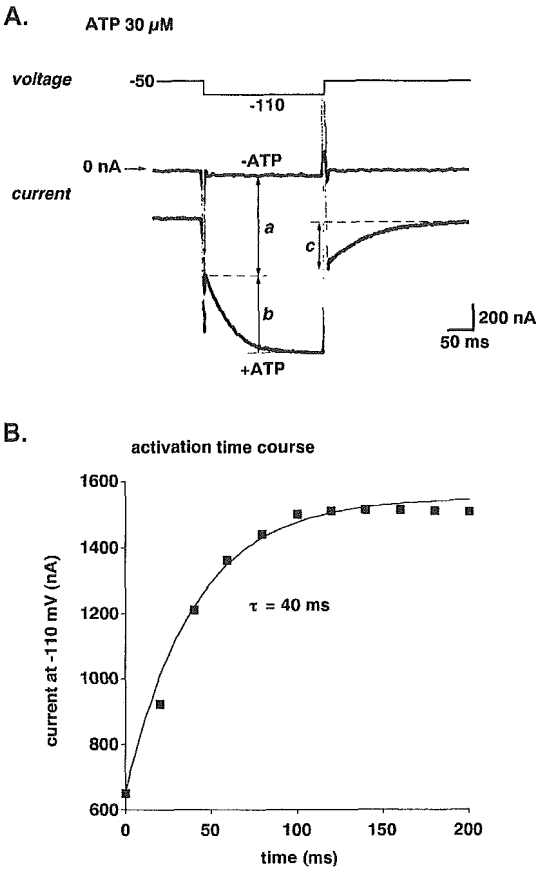

Fig. 1. (A) Current traces of an oocyte stepped to −110 mV from a holding potential of −50 mV in the absence (−ATP) or presence (+ATP) of 30 μM ATP. The current evoked by ATP is represented by the difference between the two traces. Upon hyperpolarization, a gradual increase in current was observed in the presence of ATP, suggesting activation of a voltage-dependent gate (denoted by "b"). The current denoted by "c" represents a gradually declining "tail current" that was observed when the voltage was returned to −50 mV. (B) Time course of activation of the voltage-dependent component. Current amplitude of the voltage-dependent component represented by "b" in panel A was plotted against time after the onset of hyperpolarization at −110 mV. The voltage-dependent component could be made to fit a curve with a time constant of 40 ms.

(Fig. 2C). While the current amplitude demonstrated voltage dependence (Fig. 2B), voltage did not have an effect on time course of the activation.

3.2. Effect of ATP concentrations

Fig. 3A shows the voltage-dependent component of the current activated by 10 μM or 300 μM of ATP in a single oocyte. The relative size of the voltage-dependent component involved in total ATP-evoked current became smaller when the current was evoked by greater concentrations of ATP (Fig. 3A and B). A similar dependence on ATP concentration was observed for the current evoked in the presence of 10.8 mM Ba^{2+} instead of 1.8 mM Ca^{2+} (Fig. 3B). Dependence on ATP concentrations was also found for activation time constants for the voltage-

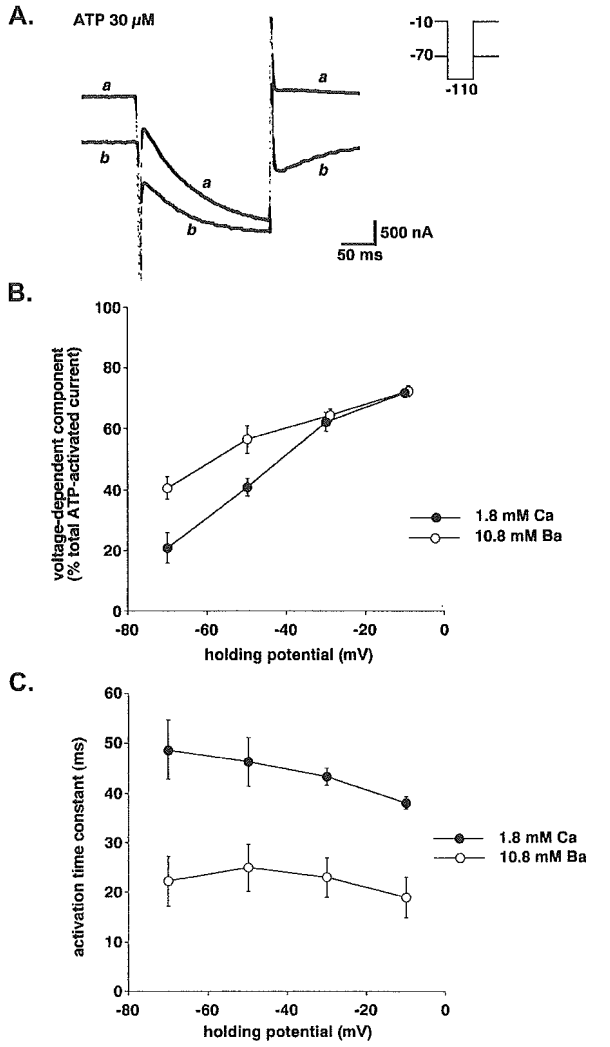

Fig. 2. Effect of holding potential on current. Current was evoked by 30 μM ATP. (A) Voltage-dependent current at −110 mV when stepped from a holding potential of −10 mV ("a") or −70 mV ("b"). (B) Effect of holding potential on voltage-dependent current. The amplitude of the voltage-dependent current was measured as described in Fig. 1A. Mean values obtained from 4 oocytes in a standard extracellular solution containing 1.8 mM Ca^{2+} (●) and an extracellular solution containing 10.8 mM Ba^{2+} (instead of Ca^{2+}; ○) were plotted. Bars represent the S.E.M. (C) Time course of activation of the voltage-dependent component. Time constants were determined as shown in Fig. 1B, and mean values obtained from 4 oocytes were plotted against holding potentials. Bars represent the S.E.M.

dependent component; the time constants were larger for 10 μM ATP than 30 μM ATP (Fig. 3C).

3.3. Activation and deactivation kinetics

Cl^- currents are observed in *Xenopus* oocytes (Weber, 1999; Zhang and Hamill, 2000). In the following experiments, current measurements were made using an extracellular solution containing 96 mM Na-aspartate instead of NaCl in order to facilitate the analysis of the voltage-dependent component of ATP-evoked current by reducing Cl^- currents. In doing so, there was an obvious reduction in outward current upon depolarization, resulting in better voltage-clamp conditions. Using this extracellular solution, the EC_{50} value for ATP-activated current measured at −50 mV was about 40 μM, which was lower than the value obtained with the standard extracellular solution containing 96 mM NaCl (about 100 μM; Nakazawa and Ohno, 2004). Fig. 4 illustrates

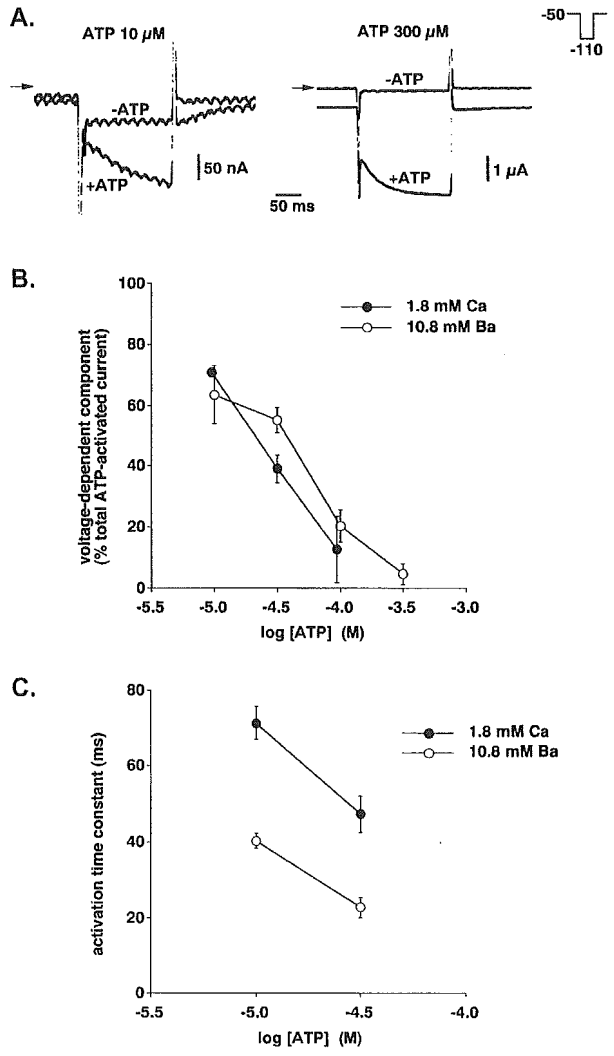

Fig. 3. Effect of ATP concentration. The voltage-dependent current was activated by hyperpolarization (−110 mV) from a holding potential of −50 mV. (A) Voltage-dependent current activated by 10 μM or 30 μM ATP. Current traces in the absence (−ATP) or presence (+ATP) of ATP are superimposed in each panel. (B) Contribution of the voltage-dependent current to total ATP-evoked current using different ATP concentrations. Mean values obtained from 4 oocytes in a standard extracellular solution containing 1.8 mM Ca^{2+} (●) and an extracelllular solution containing 10.8 mM Ba^{2+} (instead of Ca^{2+}; ○) were plotted. Bars represent the S.E.M. (C) Time course of activation of the voltage-dependent components. Time constants were determined as shown in Fig. 1B, and mean values obtained from 4 oocytes were plotted against holding potentials. Bars represent the S.E.M.

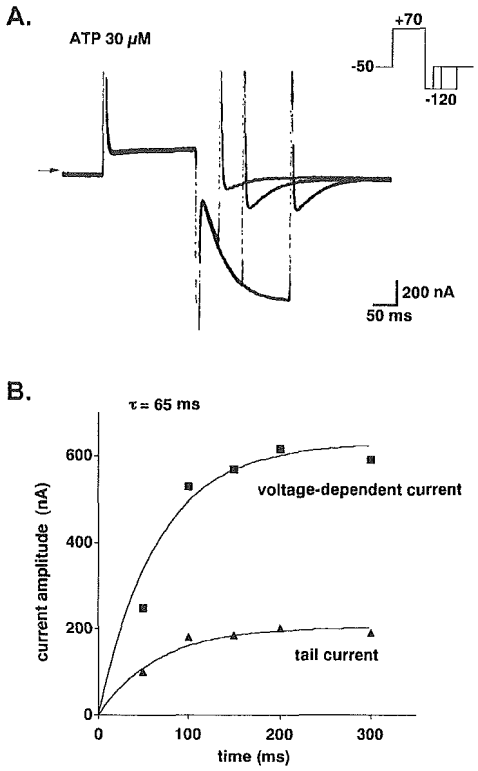

Fig. 4. Activation and tail current. (A) Gradual increase in magnitude of the tail current with increasing voltage-dependent current. Current traces obtained upon exposure to hyperpolarizing pulses (−120 mV) of different durations are superimposed. (B) Time course of activation of the voltage-dependent (■) and tail (▲) currents. Current amplitude was plotted against duration of hyperpolarization (also shown in panel A). The results of both time course activation experiments fit curves with a single time constant of 65 ms.

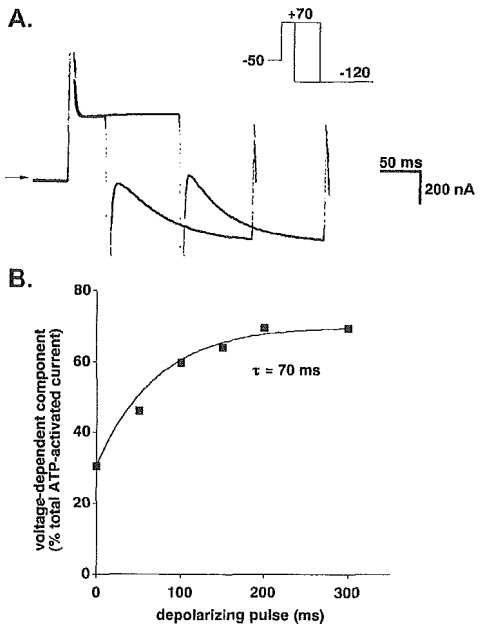

Fig. 5. Deactivation of the voltage-dependent component. (A) Current traces obtained using depolarizing pulses (+70 mV) of two different durations. The amplitude of the voltage-dependent component increased when the duration was prolonged. (B) Time course of deactivation of the voltage-dependent component. Current amplitude was plotted against duration of the depolarizing pulses (also shown in panel A).

the relation between activation kinetics of the voltage-dependent component and time course of tail current. As shown in Fig. 4A, oocytes were stepped to 70 mV and then to −120 mV to induce the voltage-dependent component. When hyperpolarization at −120 mV was terminated after various periods, a gradual increase in amplitude of the tail current was observed with increased duration of hyperpolarization at −120 mV. Time courses of both the voltage-dependent component and tail current could be fitted with curves with a single time constant (65 ms in this case; Fig. 4B). Similar fitting with single time constants were made for 4 oocytes tested, and the mean time constant±S.E.M. was 66.3±2.4 ms.

With increased duration of the +70 mV depolarizing pulse, increased amplitude of the voltage-dependent component was observed at −120 mV (Fig. 5A). This may reflect "deactivation" of the voltage-dependent component (Scheme 1):, where A is ATP, and R and R* are closed and open states, respectively, of the voltage-dependent component of $P2X_2$ receptor/channel. The deactivation time course could be fitted with a time constant of 70 ms in this case (Fig. 5B; mean±S.E.M., 71.3±1.3 ms; n=4).

3.4. Voltage dependence of activation and deactivation

As shown in Fig. 1, contribution of the voltage-dependent component to total ATP-evoked current was influenced by the holding potential prior to hyperpolarization. This was further examined by testing a number of prepulses at various potentials prior to hyperpolarization (Fig. 6A). As the prepulse became more depolarized, a greater contribution of the voltage-dependent component to total ATP-evoked current was observed, and this contribution became maximal near 0 mV (Fig. 6B). Thus, the voltage-dependent gate must be completely closed at potentials equal to or more positive than 0 mV. The data were fitted with a curve in accordance with the following model of "deactivation":

$$d_\infty = 1/\{1 + \exp[(E_{1/2} - E_m)/k]\}, \quad (1)$$

where d_∞ represents the relative proportion of closed gates at steady state, $E_{1/2}$ is the voltage at which the half-maximal closing occurs, E_m is the membrane potential, and

$$A{\cdot}R \underset{\text{(deactivation)}}{\overset{\text{(activation)}}{\rightleftharpoons}} A{\cdot}R^*$$

Scheme 1.

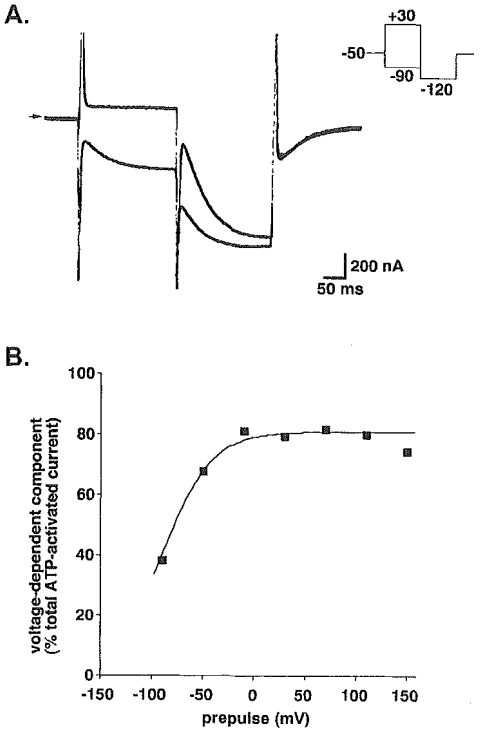

Fig. 6. Prepulse experiment. An ATP concentration of 30 μM was used. (A) Current traces obtained using prepulses of +30 mV ("a") or −90 mV ("b") prior to hyperpolarization at −120 mV. (B) Effect of prepulses. The relative contribution of the voltage-dependent current to total ATP-evoked current at −120 mV was plotted against each prepulse voltage. Some of this data is also shown in panel A.

k is a slope factor reflecting an energy barrier (Hodgkin and Huxley, 1952; Hille, 1992a). As shown in Fig. 6B, potential at which half the gates closed was estimated to be −90 mV in this case (mean±S.E.M., −78.8±5.2 mV; n=4).

The voltage dependence of activation was also examined. As shown in Fig. 7A, the channels responsible for the voltage-dependent component was sufficiently "deactivated" by applying a prepulse of +100 mV, and they were then activated at various hyperpolarization potentials. Contribution of the voltage-dependent component to total ATP-evoked current decreased as the hyperpolarization became more negative up to −45 mV in the case shown in Fig. 7B. Potentials exceeding −45 mV could not be examined since the resultant ATP-evoked current was not large enough to analyze. The data were fitted in accordance with the following model of "activation":

$$a_\infty = 1/\{1 + \exp[(E_{1/2} - E_m)/k]\}, \quad (2)$$

where a_∞ represents the degree of gate opening at steady state. The other parameters are the same as those described above. The data obtained using Eq. (2) (Fig. 7B) could be fitted with a curve indicating that half of the gates were open at a potential of −30 mV.

The above data suggest that activation of the voltage-dependent gate occurs at more positive potentials than gate deactivation. To further investigate this, the fraction of the gates that escaped deactivation ($1-d_\infty$) was calculated from the data obtained during deactivation experiments. The deactivation data was then plotted alongside data obtained from activation experiments (Fig. 7C). These data suggest that the activation potential is 50 mV more positive than the deactivation potential.

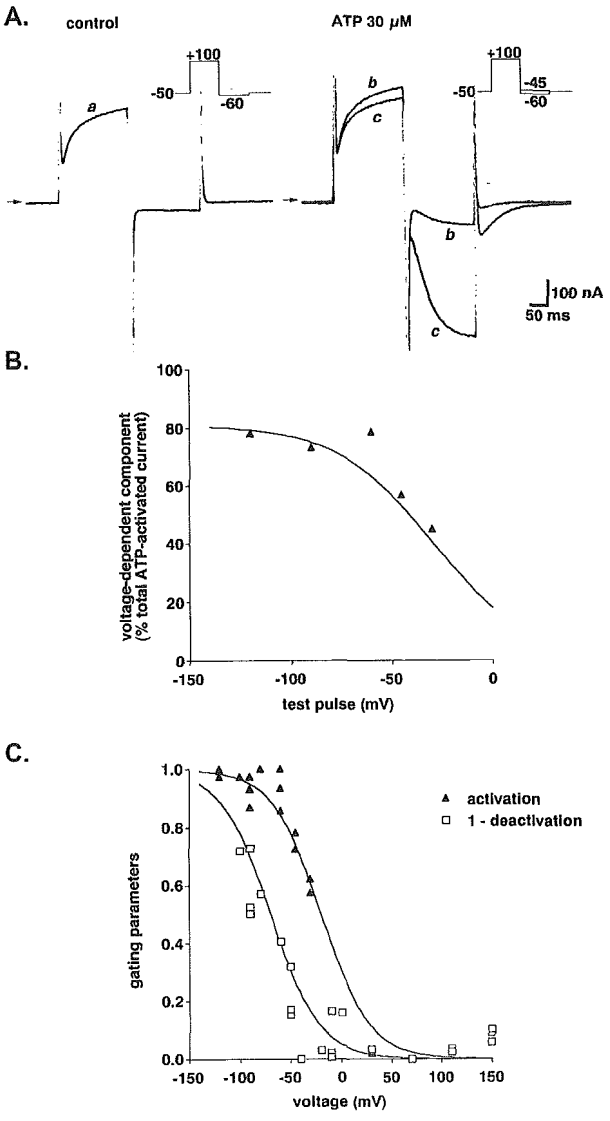

Fig. 7. Effect of hyperpolarization on voltage-dependent current. (A) Current traces before (control) and during the application of 30 μM ATP. In the panel on the right, two current traces obtained following hyperpolarization at −45 mV ("b") and −60 mV ("c") are superimposed. (B) Contribution of voltage-dependent current to total ATP-evoked current at various hyperpolarization potentials. Some of these data are shown in panel A. (C) Comparison of activation and deactivation. Parameters describing activation and deactivation were determined as described in the text. Each data point represents data obtained from individual oocytes.

4. Discussion

4.1. Schematic model of voltage-dependent gating

Recombinant $P2X_2$ receptor/channels expressed in *Xenopus* oocytes exhibited voltage-dependent gating properties similar to those of the channels in PC12 cells (Nakazawa et al., 1997b). The following similarities were observed: (1) the gate opens at negative potentials, (2) activation follows a time course with a time constant of 40 to 70 ms, and (3) gating depends on ATP concentrations. Thus, voltage-dependent gating in PC12 cells may be due to intrinsic expression of $P2X_2$ receptor/channels. We depict here a model that has been proposed to explain voltage-dependent gating of the channels in PC12 cells (Scheme 2):, where A is ATP, R_L and R_H represent closed states, and R* represents the open state (Nakazawa et al., 1997b). In this model, voltage-dependent gating is explained by transition between low and high ATP-affinity states. Upon hyperpolarization, there is a shift from the R_L to the R_H conformation. ATP preferentially binds to channels in the R_H state ($A \cdot R_H$), after which the channels open ($A \cdot R_H^*$). Binding of ATP is the rate-limiting step since activation kinetics were observed to depend on ATP concentrations in the present study (Fig. 3C). The following rate constants have been proposed (Scheme 3): where k_{+1} parallels the concentration of ATP ($k_{+1}=k'_{+1}$[ATP]), and K_d is given by k_{-1}/k'_{+1} (Hille, 1992b). In the present experiment, an activation time constant of 65 ms was observed in the presence of 30 μM of ATP (Fig. 4), which is equivalent to a rate constant of 15 s^{-1}. Using these values, $k'_{+1}=k_{+1}/[ATP]=15\ s^{-1}/(30\ \mu M)=5\times10^5\ M^{-1}\ s^{-1}$. An inactivation time constant of 70 ms was observed in the presence of 30 μM of ATP (Fig. 5), which is equivalent to a rate constant of 14 s^{-1}. Thus, K_d was calculated to be $k_{-1}/k'_{-1}=14\ s^{-1}/(5\times10^5\ M^{-1}\ s^{-1})=28$ μM, which is slightly less than the EC_{50} value obtained at −50 mV (about 40 μM). This estimation is in accordance with the finding that the voltage-dependent component is not completely activated at −50 mV (Fig. 7C). It is difficult to quantify the low-affinity ATP binding state since the relationship between concentration and response needs to be assessed at highly positive potentials, while $P2X_2$ receptor/channels permit only small current due to their inward-rectifying nature. We estimate here the low affinity from simple theoretical concentration–response curves. Fig. 8 shows two concentration–response curves. One demonstrates an EC_{50} of 30 μM, corresponding to a high-affinity state. If the other low-affinity state demonstrates an EC_{50} of 100 μM, more $P2X_2$ receptor/channels were in the high-affinity state in the presence of 10 μM ATP, and more were in the low-affinity state in the presence of 300 μM ATP. This is consistent with the greater observed contribution of the voltage-dependent component to total ATP-evoked current in the presence of 10 μM, while little was observed in the presence of 300 μM ATP (Fig. 3). Thus, the low-affinity state may be lower than the high-affinity state by threefold or larger.

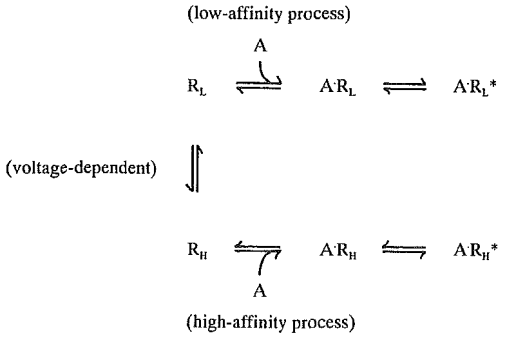

Scheme 2.

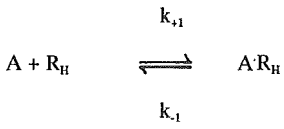

Scheme 3.

The idea of the transition of $P2X_2$ receptor/channels between low- and high-affinity states might explain the "non-voltage-dependent" component of ATP-evoked current. For example, the current evoked by 30 μM ATP was not completely observed as voltage-dependent component even when activated at very negative potentials (Fig. 7B) or following deactivation at very positive potentials (Fig. 6B). This "non-voltage-dependent current" (about 20% of the total ATP-evoked current) might result from the activation of $P2X_2$ receptor/channels in the low-affinity state prior to voltage-dependent activation.

The voltage dependence of activation and deactivation differed, with deactivation occurring at more negative potentials (Fig. 7C). This indicates that the activation and the deactivation do not arise from a simple reversible "back-and-forth" process, rather, two voltage-dependent processes

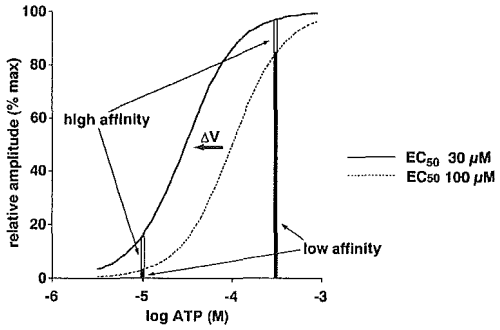

Fig. 8. Voltage-dependent change in sensitivity to ATP might explain dependence of the voltage-dependent current on ATP concentration. Low-affinity (EC_{50}=100 μM) and high-affinity (EC_{50}=30 μM) states of the receptor are thought to exist (Hill coefficient; 1.5). Each receptor shifts from a low-affinity to a high-affinity state upon hyperpolarization (ΔV). With 10 μM ATP, only a small proportion of the receptors, many of which were in the low-affinity state, were activated prior to hyperpolarization, but many more were activated upon induction of the high-affinity state by hyperpolarization. In the presence of 300 μM ATP, a larger proportion of the receptors were activated even in the low-affinity state, and induction of the high-affinity state caused only a marginal increase in activated receptors.

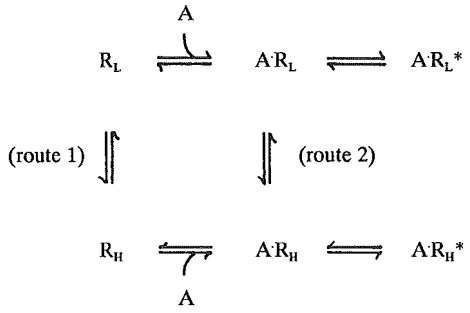

Scheme 4.

may be involved. We propose the following modification to Scheme 2.

This model (Scheme 4) involves two voltage-dependent processes, one resulting in activation through "route 1", and the other resulting in deactivation through "route 2". Such model would explain the observed difference in voltage dependence between activation and deactivation. However, we would expect this model to result in more difficult to interpret data than we did above based on Schemes 2 and 3.

4.2. Relevance of voltage-dependent gating

$P2X_2$ receptor is expressed in a number of neurons (e.g., Atkinson et al., 2000; Rubio and Soto, 2001). $P2X_2$ receptor/channel is permeable to Ca^{2+} (Egan and Khakh, 2004), and Ca^{2+} influx through the channel may influence cellular activity, although its exact role remains to be clarified. The voltage-dependent gating reported here may be relevant to the Ca^{2+} influx from the following consideration. Na^+ current (I_{Na}) and Ca^{2+} current (I_{Ca}) permeating through $P2X_2$ receptor/channel are:

$$I_{Na} = -P_{Na}\frac{E_m F^2}{RT}\frac{[Na]_o}{1-\exp(-EF/RT)} \quad (3)$$

$$I_{Ca} = -4P_{Ca}\frac{E_m F^2}{RT}\frac{[Ca]_o \exp(-2EF/RT)}{1-\exp(-2EF/RT)}, \quad (4)$$

where P_{Na} and P_{Ca} represent the permeability of Na^+ and Ca^{2+}, respectively, E_m represents the membrane potential, and F, R, and T are their usual physicochemical meanings (Fatt and Ginsborg, 1958; Nakazawa et al., 1989). The ratio of I_{Na} to I_{Ca} is thus:

$$\frac{I_{Ca}}{I_{Na}} = \frac{4P_{Ca}[Ca]_o}{P_{Na}[Na]_o}\frac{1}{\exp(E_m F/RT)[\exp(E_m F/RT)+1]} \quad (5)$$

This equation indicates that the ratio of I_{Ca}/I_{Na} is larger at more negative potentials. The ratio calculated at −90 mV is about 13-fold larger than that calculated at −30 mV. Thus, channel opening at negative potentials favors Ca^{2+} over Na^+ influx. Thus, voltage-dependent gating may facilitate cellular Ca^{2+}-dependent responses when cells are hyperpolarized. This may occur when efflux through K^+ channels outpaces depolarization afforded by opening of $P2X_2$ receptor/channels.

4.3. Conclusion

The results of the present study suggested that $P2X_2$ receptor exhibits voltage-dependent gating, and that this is not due to simple activation and deactivation of a single gate, but rather, due to a transition from a low ATP affinity to a high ATP affinity state. This may favor Ca^{2+} influx at negative potentials, although further studies are required to clarify the physiological significance of voltage-dependent gating of $P2X_2$ receptor.

Acknowledgements

This work was supported, in part, by a Health and Labour Science Research Grant for Research on Advanced Medical Technology from the Ministry of Health, Labour and Welfare, Japan, as well as a grant-in-aid for scientific research from the Ministry of Education, Science, Sports and Culture, Japan (KAKENHI 13672319) awarded to K.N.

References

Atkinson, L., Batten, T.F., Deuchars, J., 2000. $P2X_2$ receptor immunoreactivity in the dorsal vagal complex and area postrema of the rat. Neuroscience 99, 683–696.

Brake, A.J., Wagenbach, M.J., Julius, D., 1994. New structural motif for ligand-gated ion channels defined by an ionotropic ATP receptor. Nature 371, 519–523.

Clyne, J.D., LaPointe, L.D., Hume, R.I., 2002. The role of histidine residues in modulation of the rat $P2X_2$ purinoceptor by zinc and pH. J. Physiol. 539, 347–359.

Egan, T., Khakh, B.S., 2004. Contribution of calcium ions to P2X channel responses. J. Neurosci. 24, 3413–3420.

Egan, T.M., Haines, W.R., Voigt, M.M., 1998. A domain contributing to the ion channel of ATP-gated $P2X_2$ receptors identified by the substituted cysteine accessibility method. J. Neurosci. 18, 2350–2359.

Ennion, S., Hagan, S., Evans, R.J., 2000. The role of positively charged amino acids in ATP recognition by human $P2X_1$ receptors. J. Biol. Chem. 275, 29361–29367.

Fatt, P., Ginsborg, B.L., 1958. The ionic requirements for the production of action potentials in crustacean muscle fibres. J. Physiol. 142, 516–543.

Haines, W.R., Migita, K., Cox, J.A., Egan, T.M., Voigt, M.M., 2001. The first transmembrane domain of the P2X receptor subunit participates in the agonist-induced gating of the channel. J. Biol. Chem. 276, 32793–32798.

Hille, B., 1992a. Classical biophysics of the squid giant axon. Ionic channels of excitable membranes, Second Edition. Sinauer, Sunderland, MA, pp. 23–58.

Hille, B., 1992b. Ligand-gated channels of fast chemical synapses. Ionic channels of excitable membranes, Second Edition. Sinauer, Sunderland, MA, pp. 140–169.

Hodgkin, A.L., Huxley, A.F., 1952. The dual effect of membrane potential on sodium conductance in the giant axon of *Loligo*. J. Physiol. 116, 497–506.

Jiang, L.H., Rassendren, F., Surprenant, A., North, R.A., 2000. Identification of amino acid residues contributing to the ATP-binding site of a purinergic P2X receptor. J. Biol. Chem. 275, 34190–34196.